March 2018

Authors' response to reviews

Authors: Johanna Kerch, Anja Diez, Ilka Weikusat and Olaf Eisen

Title: Deriving seismic velocities on the micro-scale from c-axis orientations in ice cores

Please note:

- Authors' response in **bold.**
- Our changes are in blue, also in the corresponding new manuscript (old: red).
- Line numbers mentioned here refer to the reviewed manuscript.

Response to referee #1, Maurine Montagnat

Overall, the paper is very nicely written and well organised. Descriptions of the different tools, and different steps are very clear, an easy to read. I will therefore have mainly one main comment, about the purpose of the work and the way it is provided through the text.

We thank Maurine Montagnat for her valuable discussion and detailed comments for improving our manuscript.

As mentioned in the summary, the purpose of using seismic or sonic data to explore ice anisotropy development in ice sheets and glaciers is to be able to (i) avoid using the long and small-scale technique of thin-section + analyser, (ii) to provide data including larger volume of ice and therefore more representative, and (iii) to perform more measurements, over larger areas. (There might exist other interests, but these ones are already strong). To do so, one needs to be able to invert the seismic signal into a texture data. The best would be to have access to the full orientation of every grain (c- and a-axes). In the "real life", we will mainly have access to some "symmetry" of the texture, at a polycrystalline scale, over a given volume. A symmetry that is associated with the tool used (radar...) and the inversion procedure. This is likely why previous works mentioned in the text focused on the eigenvalues of the second orientation tensor, with some symmetry hypotheses, as the likely result of this inversion. But there is no hope that this inversion could give access to the exact c-axis orientation distribution over this volume (as far as I know from the available equipment so far). Therefore it should be made very clear that the work performed in this paper is an exercise aiming at pointing the likely error deriving from the inversion procedure in some specific cases. Otherwise, making use of an existing c-axis distribution data set to obtain seismic velocities has no interest by itself. Therefore how the given algorithm (cx framework) will help to improve the inversion procedure should be made clearer in the text. For instance, could a shear-wave splitting from a seismic dataset could be directly inverted as resulting from a non-symmetric orientation distribution (cf. Abstract), and provide some information about this orientation distribution? From the comparison between the ev and cx framework performed here as an "exercise", could some specific signal be obtained to be able to assess that an experimentally obtained seismic signal is related to a non vertically clustered fabric (as in the case of the bottom of KCC)?

We agree that it is very unlikely that an application of an inverse method will be able to reproduce a full crystal orientation distribution. However, our work not only aims at pointing at the error made by various approximations and is not intended for inversion purposes. Instead, we demonstrate the effect of a real fabric on seismic velocities which should be of special interest to the seismologic community. Our results may call for a reassessment of seismic velocity analysis without the inverse process being the necessary motivation, but obviously an additional opportunity to apply various frameworks.

Even though the presented framework is not suitable for inversion, we can use it for the

forward calculations. To understand the variations of seismic velocities caused by variations in the crystal orientation fabric we need to be able to calculate these seismic velocities as correctly as possible. Therefore, the important objective of this study is to convey our better understanding of the distribution of seismic velocities in ice achieved so far. As we are not trying to aim for an inversion of seismic velocities to a full crystal orientation tensor we do not perform an exercise trying to derive the full crystal orientation distribution from seismic data. It is simply beyond the scope of the paper.
We included in the introduction:
Our main objective is to present an improved method for the estimation of the bulk elasticity tensor, and to use this to (i) evaluate the use of the *ev* framework, and (ii) demonstrate the effect of a real fabric on seismic velocities. Our study concentrates on the forward calculation of seismic velocities from the full crystal orientation distribution. The application of an inverse method will likely always require some simplification to symmetries, for which we now can quantify involved uncertainties – a required component of the covariance matrices for inverse methods.

In the discussion part, the authors should make it clear how their work can be used to provide "safeguards" against misinterpretation of the seismic signal by a "simple" inversion toward an eigenvalue data set.
Like mentioned before, the aim of this paper is not to provide a method for inversion, but rather increase our understanding of seismic velocity distributions caused by variations in the crystal orientation distribution. Therefore, we try to increase awareness for the simplifications being made by using symmetry distributions or eigenvalues to describe seismic velocities caused by crystal anisotropy. This is the first paper where we go beyond the study of these symmetries. Setting safeguards would require a full understanding of the possible distributions and a classification of these again into some kind of symmetries or clusters, something we are avoiding by calculating velocities from the full crystal distribution. We therefore see the aim of this paper in increasing awareness and understanding of seismic anisotropy in ice rather than creating another classification scheme.
Nevertheless, we add a statement in the discussion of the cx framework:
Potentially, our framework can be used in principle for the development of inverse methods to derive the fabric distribution from seismic velocities. Following experience from other fields of active seismology, this would, first, most likely require comprehensive data sets suitable for full-waveform inversion not yet available for glaciological applications; and, second, some simplifying assumptions on the distribution of crystal fabric, e.g. in terms of considered symmetries. The framework we presented allows to quantify the potential effect of simplifying assumptions and could help to more accurately specify covariance matrices, thus enabling the quantification of uncertainties coming along with the results produced by application of an inverse method.

Another important point that the authors should mention is that, contrary to the c-axis orientation angles, the eigenvalues of the second order orientation tensor do not provide a complete and unambiguous description of the texture. Indeed, one would require all the other orders of this orientation tensor to do so. By working with eigenvalues, we already work with an incomplete and bias COF data. Therefore, some variability are strongly smoothed by this procedure. Indeed, a multi-cluster type of texture will appear like a cone-angle type with the eigenvalue data, while the c-axis orientation distribution will give access to the complexity. So this is not such a result to find that the variability is better reproduced by using directly the full c-axis data...
This is correct, the variability in seismic velocities is higher using the full crystal orientation distribution than using eigenvalues. However, this is the first study to actually use the full information to extract and demonstrate the variability. This is what we consider a noteworthy result.
We added to section 2.3, uncertainty of the *ev* framework:
The eigenvalues of the second-order orientation tensor do not constitute a complete and unambiguous

description of the fabric. Specifically, they do not provide information on preferential orientations with regard to the coordinate system.

One more point, that seems to me important but that could result from a misunderstanding from my side: The eigenvalues are provided together with the set of eigenvectors. The orientation of these eigenvectors provide the "orientation of the fabric" (if we can call it that way) relative to the thin section referential... Let's assume the thin section was done with a very strict control so that it's orientation relative to the "real" vertical is very well known, and that the core can be assumed to be vertical, then, the orientation of the eigenvector referential should tell us about some "non verticality". By making the assumption that this referential corresponds somehow to the "real" vertical, one introduce a strong assumption. This is hard to do otherwise, because of all the unknown mentioned before. BUT this assumption is not made at all when using the cx framework, since the true orientations are considered, and these orientations could be titled relative to the "real" vertical because of a tilted core, or during the thin section process... We can then expect some bias in the comparison due to this difference of consideration of this "tilt" of the fabric. This is mentioned somewhere within the text, but it does not appear to be considered as a source of differences between the velocity measurements, although is could play a strong role, especially along the KCC core. Shouldn't it be tested? For instance by aligning systematically the incidence angle with the eigenvector relative to the largest eigenvalue?

We make the assumption that the ice core axis is vertical (and discuss the effect of this assumption later) and that this axis is also the reference for the c-axis angles from the thin sections. These are the basis for calculating the eigenvalues. The ev framework works on the assumption that the eigenvector of the largest eigenvalue coincides with the vertical, without any additional information. This introduces an error when calculating seismic velocities from the ev framework. However, this is part of the errors that are introduced by the ev framework and we therefore do not want to correct for this artificially. Regardless of any tilt of the ice core axis relative to the (gravitational) vertical we compare the two frameworks within the same reference system, so there should be no bias from this. We cannot see an easy way to circumvent this problem in real application, as the question of verticality and ice-core orientation in the borehole is still not fully solved from a technical point of view.

For clearification, we added to the previous addition in section 2.3:

To get a rough idea about the orientation of the fabric the eigenvectors would have to be used in addition, an approach seldomly followed. Instead, the orientation of the eigenvector to the largest eigenvalue is typically assumed to correspond to the vertical, which may in fact not be the case and could introduce an unknown uncertainty.

And the end, about the discussion corresponding to the layering of the core (discussion part). Couldn't this cx framework be perfectly adapted to test the effect of such a layering on a seismic velocity data set? One could artificially vary the length of the layers, and force the anisotropy and check whether the response stands within the resolution frame of the measurements, etc. Maybe I am not qualified enough to see where the difficulty stands but it would be a nice byproduct of this cx framework?

This is correct, next steps following our study could and should include the modelling of synthetic seismograms to assess the effect (conclusion). However, modelling synthetic seismograms for the anisotropic case is not straight forward and would go way beyond the scope of our paper. As an example, we would like to point out to the reviewer the progress made in modelling synthetic radargrams by Eisen et al. over the last decades, which is a much simpler physical problem than the propagation of elastic waves, but still not adequately solved. The development of such a forward algorithm for elastic wave propagation is of course desirable, as it would also mark the first step to develop decent inverse methods to retrieve the fabric distribution from seismic observations.

P1 L20: Please site previous works done on that, or mention that Faria et al. is a review.
We noted that Faria et al. (2014) is a review paper.

Section 2.4, P7 L5: Maybe remind here that you are entering the cx-framework.
We added: We refer to the new approach as *cx* framework.

P7 L1-2: the authors refer to the error introduced in the ev framework, as if it was interesting "by itself", while it should be put back in the context of the inverse approach that aims at going from seismic data to eigenvalues (since going to real c-axis measurements will not be possible). What is the amount of signal lost? What kind of mistake could be made?? Is this inversion making sense? This is why the cx framework could be really meaningful.
We are not sure whether we understood this comment correctly, apologies if we did not. We agree that the cx framework is important and meaningful in terms of the inversion of seismic data to gain information about crystal anisotropy. However, as stated above, the scope of this paper is not the application of an inverse method to seismic data but a better understanding of the variations in seismic velocity caused by crystal anisotropy and the errors that are introduced by using simplified symmetries for the description of anisotropy. Therefore, the *ev* framework helps to increase our understanding of seismic velocity variations and is important to discuss by itself.

P8 L8: **Appendix 1A refers to Tsvankin. As we are repeating it in Appendix B of our paper we removed the confusing reference.**

P9 L4-5: here I started questioning myself about the effect of a non vertical texture that is translated into "non vertical" eigenvectors (to say it simply, see previous remarks), and that could have some impact by not being considered into the ev framework, but well integrated, per-se, into the cx framework.
See above explanation.

P11 L3: how many layers do you use for the RMS calculations? How to you choose them? How does this impact the result? Same question for the case of KCC data treatment.
For EDML we use all available data for the calculation without a selection and center the layers around the data points. We have no information on which layers could be more dominating, which is why we do not make any additional assumptions. The average layer thickness is 16 m. For KCC we first calculate the average speed in each continuous measurement interval (as explained in the text) and then extend the layers to half the distance to the neighboring intervals (12 layers).

P11 L14: maybe put here "change in the estimated variation of seismic velocities", since these velocities are modelled and not measured... By the way, what is the resolution expected in the seismic velocity measurements? Are the differences evidenced here above or below these resolutions?
The sentence you are referring to was deleted on the 2nd reviewer's request. The resolution of conventional surface based seismic surveys is lower than the fabric-based seismic velocity variations (see conclusion).

P13 L7: OK theoretically, but in general we don't know where is the exact vertical when analysing thin sections, and it can be tilted more than 10°, either because of inclined drilling, or because of thin section processing, or both...
You are of course right that a drilling inclination would mean that ice core axis and vertical diverge. Ideally, a known borehole inclination would be part of our framework (and any thin section analysis), but then there is still the problem of the ice core orientation, which would

also be needed for a correction. (We think we can safely neglect the thin section processing as contribution to this uncertainty as it is a standardised procedure starting from the sawing of the ice core.) Therefore, without further information, we make the assumption that ice core axis and vertical coincide (section 2). A possible inclination does not eliminate the ability of our cx framework to resolve the azimuthal variation of a non-symmetrical c-axis distribution. However, we did not mention this additional source of uncertainty before and added in the discussion of azimuth-sensitive seismic velocities:
The appearance of a non-symmetric fabric might also be induced by inclined drilling. Ideally, to be able to link calculated and measured seismic velocities a possible inclination of the ice core with respect to the vertical and to the horizontal seismic profile should be considered.

P15 L15: about the likely misinterpretation, maybe give an illustration in the data, for clarity?
A new figure (see next comment) illustrates that in several depths the velocity in dependence of the incidence angle appears shifted from the neighboring samples. This could be caused by the misorientation of neighbouring ice core pieces or it could be a true variation. We wanted to alert the reader to be aware of this issue. The specific depth, where the core orientation appears lost (1705 m), is based on the Schmidt diagrams (not shown) but this could be the case for more depths. We included a remark in the caption of the new figure pointing it out.

P16 L6: maybe put the figure in appendix at least, I was quite frustrated not to see it...
Sorry for that, we did not want to cause any unnecessary frustration but did not include the figure in the beginning for length constraints. However, as per your request, we now included the figure in section 3.2 (Fig. 10) showing P-wave velocity difference between the frameworks and azimuthal change for EDML.

P17 L2: "The cx framework provides a refined approach for the use of fabric information to obtain seismic velocities in ice"... Once again, what we aim at is to obtain the fabric out of seismic data (unless there exist other purposes that should be mentioned!). So what can we learn out of this "exercise" that could help to solve the inversion problem, and to be more accurate in treating seismic data in terms of fabric information???
Thanks for your comment. As mentioned before the aim of the ev framework is not to apply an inverse method to seismic data. We know that one of the main goals will be to derive reliable information about crystal anisotropy from seismic data and this will only be possible using simplified symmetries, however, to be able to do so reliably we have to understand the system and possible errors. Therefore, the cx framework is in itself important to gain reliable and most correct information for the forward calculation of seismic velocities in anisotropic ice.

P17 L24-29: I find this paragraph highly speculative, and not necessary here... to relate stress conditions to grain bounding so quickly is speculative, and to mention the effect of GBS (that is far from being realistic along ice cores with large grain size) on elasticity is also very strong! Maybe it would be better to remain in the core of the subject?? or you would need to justify more...
We agree that this paragraph is not mandatory. However, for completeness, we want to address additional processes on the crystal scale that might play a role, especially when measuring in the laboratory. More and more studies focus on the measurement of ultrasonic velocities on ice cores to derive information of crystal orientation on the microscale in high resolution with the aim of finding better connection to the macroscale observations. Therefore, we would like to keep this paragraph with the cited papers giving the necessary context.

P18 L9: Again, OK with what is said here, but since we have no hope to be able to inverse seismic data into exact c-axis orientations, how helpful is this framework?

Like mentioned before, the study of seismic velocities in anisotropic ice should not be reduced to the only goal of an inversion scheme. Setting up a well working and powerful inversion of seismic velocities or even the full wave form requires a deeper understanding of the processes and possible variations. If we only always discuss and analyse highly simplified versions we cannot gain any more in-depth understanding of the system. In fact, we could, but to quantify the errors coming along with that we first need to understand the full approach. Therefore, if we are able to derive more accurate seismic velocities from anisotropic ice we should do so. Then, in a next step, we can simplify again such a system again to (maybe) be able to invert data, with the additional knowledge we gained from the more precise forward calculations.

Response to referee #2, Huw Horgan

Kerch et al make a useful contribution to the literature with this study of crystal orientation fabric distributions and their resulting seismic velocities. The manuscript mainly focuses on presenting a framework by which c-axis observations can be converted to representative elastic properties, which are then used to estimate seismic phase velocities. The manuscript also spends considerable time comparing the new technique, which requires detailed knowledge of the c-axis distribution, to an already established framework that uses the more readily available eigenvalue representation of the c-axis distribution. The paper is well considered and includes findings that are useful to researchers working at both the micro and macro scales. Some clarification of the text is needed. Most of my comments below are intended to improve the presentation of the study and highlight some of the implicit and explicit findings.
We thank Huw Horgan for his appreciation and detailed comments on language and content for improving our manuscript.

To improve accessibility a flowchart type figure showing both the ev and cx framework would be a useful addition. The topic is necessarily dense, and the distinctions, while clear in the text, would be more instantly apparent in a figure. This would make it clear to the casual reader what is required as inputs, and what are the key steps that influence the result.
We prepared a flowchart type figure (new figure 2 in the revised manuscript) and added it to section 2.4. We added to section 2.4:
Both frameworks are summarised in Figure 2.

Furthermore, to improve accessibility, Figure 1 could be thoroughly described in the introduction. This description could include details on the seismic acquisition reference plane currently described in section 3.2. Doing this would link the scales considered in the introduction.
We moved the explanation of the seismic plane from section 3.2 to the introduction. The entire paragraph now reads:
Currently, the development and extent of fabric anisotropy is mainly investigated by laboratory measurements on ice core samples which provide one-dimensional data (along the core axis, z-axis in Fig. 1) that only partially cover the length of the core. However, geophysical evidence of crystal-orientation fabric can also be obtained by exploiting the elastic anisotropy which influences the propagation of seismic waves in ice (Blankenship et al., 1987; Smith et al., 2017). Seismic waves propagate between a seismic source and the seismic receivers on the glacier surface within the seismic plane (Fig. 1). This is the vertical plane underneath the horizontal seismic profile, which runs along the surface of the glacier, and may also contain the vertical ice core axis, along which fabric information is collected.
Seismic reflections occur due to sudden changes of fabric (Horgan et al., 2008, 2011; Hofstede et al., 2013) and offer the chance to obtain spatially distributed information on the COF structure in various depths of the ice column, the acquisition of which would be unfeasible using direct sampling via ice-coring.

The abstract needs some work. Mainly, it should include the key findings of the study. At present it details what will be presented but does not provide summary information of the main findings regarding the impact of azimuth, the degree of shear wave splitting, etc. Quantifying key findings in the abstract would be appropriate.
We changed the abstract to provide summary information of the main findings.
Comments on P1 L1-10 are included in the rewritten abstract.
Please note the rewritten abstract in the revised manuscript.

The title could benefit from rewording. One of the aims of this work is bridging the gap between the micro and macro scales in various ways. Your results inform both the micro scale and, through RMS velocities, the macro scale. To reflect this and to increase the audience consider something like: "Deriving micro to macro-scale seismic velocities from ice core c-axis orientations"
We like the new title suggestion:
Deriving micro to macro-scale seismic velocities from ice core c-axis orientations

All comments referring to a specific page and line which are not detailed below were changed in the manuscript as suggested.

Introduction

P1 L16: Elaborating on this point would be useful.
Changed to: ...evident and described on a macro-scale as most observations rely on remote sensing or ice sheet modeling.

P2 L17: **changed to:** ...the polar ice core EDML (European Project for Ice Coring in Antarctica in Dronning Maud Land).

P2 L22: 'effect' to 'affect'
Not changed, we think 'effect' is the correct term here:
Finally, we assess the effect of asymmetrical fabric distributions...

P2 L26: 'KCC' define on first usage.
Not changed: KCC is simply the name for this ice core to fit into a pattern (KCI further down the flowline and CC ("Climate/Chemical Core") on the same altitude but on a flowline on the other side of the saddle). We think that there is no benefit for the reader to have this explained.

Methodology

P4 L3: This sentence should state how and by whom.
Changed to: ...the components of the elasticity tensor were measured in the laboratory by means of Brillouin spectroscopy (Gammon et al., 1983).

P5 L2: '...is often used (cite), and we use this approach here.'
Changed to: ... is often used (Nanthikesan and Sunder, 1994; Bons and Cox, 1994; Helgerud et al., 2009; Vaughan et al., 2016), and we also use this approach here.

P5 L12: 'with the density ρ' 'where ρ denotes density, U denotes...'
Not changed: We would prefer to keep the definitions as short as possible.

P7 L11: 'hundred to a thousand' is this accurate for the lowest parts of the cores?
The number of grains is highly variable throughout the KCC core with a minimum number of 155 in medium parts of the core, a maximum of 1707 grains and more than 250 grains per section in the lowest 5 m. For EDML the number of grains is between 48 and 648 with 27 samples with less than 100 grains, 24 of which are from the depth interval 2300-2380 m, but not in the deepest part.
We added a similar sentence in the manuscript:
Specifically, for EDML the number of grains is mostly between 100 and 650 grains per sample with the exception of some large-grained samples from the depth interval 2300 − 2380 m with less than 100 grains. For KCC the number of grains is between 155 and 1707 grains per sample and there are more than 250 grains in the lowest 5 m of the ice core.

P8 L17: "by -1.5 to 0.5%" clarify what this range refers to. It's velocity differences, but state which framework is faster and what the range represents.
Changed to: The strongest velocity deviation between the frameworks is found for cone angles of approximately 50-60° at vertical incidence, where the *ev* velocity exceeds the *cx* velocity by approx. 50 m/s (absolute deviation of 1.5 %).

From ice core fabric to seismic velocities – case studies

P10 L8: Consider indicating this with an annotation on the figure.
We included an additional depth annotation in Figure 4.

P11 L9-10: Include example studies.
Changed to: Only in recent ice core projects have fabric measurements covered continuous intervals (ongoing measurements at the site of the East Greenland Ice-Core Project (EGRIP); North Greenland Eemian Ice Drilling (NEEM), Eichler et al., 2013), providing new information on fabric variability.

P11 L13: Not really the place for this kind of statement, which is more suited to the introduction or the discussion.
We removed the statement as we have a similar statement already in both abstract and conclusion.
Just to be clear, the COF observations at depth are based on 100's–1000's of grains?
See explanation for P7 L11.

P12 L1: 'The fabric data is discussed in detail in a forthcoming publication (in preparation).' This sentence is not useful. Perhaps a pers comm reference is what is needed here.
We changed the paragraph to:
We show the results of the velocity calculation for vertical incidence from the KCC fabric data in Fig. 6. The cone angle calculated from the eigenvalues varies between 10-30° for each depth interval (Fig. 6a). A detailed discussion of the fabric data is beyond the scope of this paper.

P16 L9: Define this depth range.
We added: ...upper part (0-800 m).

Discussion

P16 L14: This stand alone sentence is awkward and not a good way to begin the discussion.
We moved the sentence to the end of the first paragraph of section 3 (From ice core fabric to seismic velocities – case studies).

P18 L26: This is an obvious application for borehole televiewing (optical and/or acoustic.)
We assume you refer to e.g. Hubbard et al. (2008) who discussed "digital optical televiewing of ice boreholes". To our knowledge this has not been employed to deep boreholes (below 1500 or 2000 m, with problems below because of sealing tightness, although deeper tests at NEEM were tried) and there are some issues with the available instruments regarding the operating temperature in polar environments. We chose not to include a discussion of possible solutions to the problem of oriented vertical drilling other than the implications of our results.

P19 L15: 'over longer horizontal' specify distance scale (e.g. 10s of km)
Changed to: ...over longer horizontal distances of several kilometres.

P19 L25: It would be worthwhile to include some recommendations for field acquisition seismics. For example S-waves are not routinely acquired, should they be. Are single line orientations sufficient, or single crossings adequate?
Changed to: Following the findings of our study we recommend for seismic data acquisition in the field to (1) consider polarimetric survey setups (with two or even more crosslines) with both reflection and wideangle measurements, and to (2) focus on accurate traveltime recordings at high source frequencies. This should be supported by 3-component vertical seismic profiling where boreholes are available. Also, S-waves should be acquired as they provide useful information on crystal anisotropy due to shear-wave splitting.
On the crystal scale, we suggest to include the investigation...

Figures

Figure 1: Describe source and receiver annotations in caption.
To the caption we added:
The star symbolises the seismic source and the triangles represent a line of seismic receivers.
In general it would help the reader if this figure was more comprehensively described in the text.
In addition to the description of the seismic plane in the introduction we added in section 2.1 (this is partially repeated in section 2.2):
Figure 1 illustrates the geometric relation between the angles for describing the c-axis orientations from an ice core and the setup of a seismic survey profile across an ice core. The incidence of a seismic wave on an ice sample is determined by the angle of incidence \psi and the azimuth angle \theta_s of the seismic plane.
We also simplified the layout of Figure 1 without changing the content.

Figure 5: It would make sense if panel a was the same as Figure 3a.
We agree with your suggestion. However, the eigenvalue data for KCC is not published yet (paper in preparation), which is why we would prefer not to already show the data here.

Figure 6: Phase angle and incidence angle are used interchangeably. Better to pick one.
We picked angle of incidence **for figures 6, 7 and 8 and also changed the term in the text (3 x).**

Tables

'Reading example (*):' Not sure what this refers to, clarify.
The asterisk marks one line in the table (we moved it to the front of the line) to give an example as to how to read the table. To distinguish this further from the table caption we moved the example to be a table footnote.
We also clarified in the table caption that all extreme values are given for incidence values of 0–70° and corrected the extreme values for S-wave difference between the frameworks accordingly (before: extreme values for 0 – 90°, where the extreme values were found for angles > 70°).

References

P25 L20: This reference no longer has a clear path to publication. I suggest it is referred to as a pers comm if needed.
We agreed on a pers. comm. reference with D. Prior.

Deriving micro to macro-scale seismic velocities ~~on the micro-scale~~ from ice core c-axis orientations~~in ice cores~~

Johanna Kerch[1,2], Anja Diez[3], Ilka Weikusat[1,4], and Olaf Eisen[1,5]

[1]Alfred Wegener Institute Helmholtz Centre for Polar and Marine Research, 27568 Bremerhaven, Germany
[2]Institute of Environmental Physics, Heidelberg University, 69120 Heidelberg, Germany
[3]Norwegian Polar Institute, Tromsø, Norway
[4]Department of Geosciences, Eberhard-Karls-University Tübingen, 72074 Tübingen, Germany
[5]Fachbereich Geowissenschaften, Universität Bremen, Bremen, Germany

Correspondence to: Johanna Kerch (jkerch@awi.de)

Abstract. One of the ~~greatest~~ great challenges in glaciology ~~, with respect to sea level predictions,~~ is the ability to ~~gain information on~~ estimate the bulk ice anisotropy in ice sheets and glaciers, which is ~~urgently~~ needed to improve our understanding of ice-sheet dynamics. ~~Therefore, we~~ We investigate the effect of crystal anisotropy on seismic velocities in ~~a glacier . We~~ glacier ice and revisit the framework which is based on fabric eigenvalues to derive approximate seismic velocities by exploiting the assumed symmetry. In contrast to previous studies, we calculate the seismic velocities using the exact c-axis angles describing the orientations of the crystal ensemble in an ice-core sample. We apply this approach to fabric data sets from an ~~Alpine~~ alpine (KCC) and a polar (EDML) ice core. ~~The results allow~~ Our results provide a quantitative evaluation of the earlier approximative eigenvalue framework. For near-vertical incidence our results differ by up to 135 $\mathrm{m\,s^{-1}}$ for P-wave and 200 $\mathrm{m\,s^{-1}}$ for S-wave velocity compared to the earlier framework (estimated 1 % difference in average P-wave velocity at bedrock for the short alpine ice core). We quantify the influence of shear-wave splitting at bedrock as 45 $\mathrm{m\,s^{-1}}$ for the alpine ice core and 59 $\mathrm{m\,s^{-1}}$ for the polar ice core. At non-vertical incidence we obtain differences of up to 185 $\mathrm{m\,s^{-1}}$ for P-wave and 280 $\mathrm{m\,s^{-1}}$ for S-wave velocities. Additionally, our findings highlight the variation in seismic velocity at non-vertical incidence as a function of the horizontal azimuth of the seismic plane, which can be significant in case of non-symmetric orientation distributions and results in a strong azimuth-dependent shear-wave splitting ~~. For~~ of max. 281 $\mathrm{m\,s^{-1}}$ at some depths. For a given incidence angle and depth we estimated changes in phase velocity of almost 200 $\mathrm{m\,s^{-1}}$ for P-wave and more than 200 $\mathrm{m\,s^{-1}}$ for S-wave and shear-wave splitting under a rotating seismic plane. We assess for the first time ~~, we assess~~ the change in seismic anisotropy that can be expected on a short spatial (vertical) scale in a glacier due to a strong variability in crystal-orientation fabric ($\pm 50\,\mathrm{m\,s^{-1}}$ per 10 cm). Our investigation of seismic anisotropy based on ice-core data contributes to advancing the interpretation of seismic data, with respect to extracting bulk information about crystal anisotropy without having to drill an ice core and with special regard to future applications employing ultrasonic sounding.

1 Introduction

One of the most important goals for glaciological research is the establishment of a thorough understanding of ~~the ice dynamicsfor which the~~ ice dynamics, in which internal deformation plays a crucial role. This deformation is predominantly evident and described on a macro-scale (~~~km~~)$\mathcal{O}$(km)) as most observations rely on remote sensing or ice sheet modeling. However, it is necessary to connect the bulk behaviour with the governing processes on the micro-scale ($\mathcal{O}(\mu\text{m})$) to be able to develop a comprehensive understanding of the deformation mechanisms (Weikusat et al., 2017). The fundamental deformation mechanisms on the atomic scale are driven by the external stress field and lead to the alignment of single ice crystals in preferential directions ~~(Faria et al., 2014)~~ (previous works are reviewed in Faria et al., 2014) . Due to the intrinsic anisotropy of each ice crystal an anisotropic bulk medium is formed as a result of the crystal-preferred orientation (CPO, also known as lattice-preferred orientation, LPO, and crystal-orientation fabric, COF). The anisotropy is evident in elastic, plastic and electromagnetic properties of the ice and the respective parameters can be connected to each other. The plastic anisotropy can have a considerable influence on the bulk deformation rate and vice versa. Hence, it is desirable to incorporate the development of anisotropy in flow models ~~(Pettit et al., 2007; Seddik et al., 2008; Martin et al., 2009)~~ (Pettit et al., 2007; Seddik et al., 2008; Martin et al., Currently, the development and extent of fabric anisotropy is mainly investigated by laboratory measurements on ice core samples which provide one-dimensional data (along the core axis, z-axis in Fig. 1) that only partially cover the length of the core. However, geophysical evidence of crystal-orientation fabric can also be obtained by exploiting the elastic anisotropy which influences the propagation of seismic waves in ice (Blankenship and Bentley, 1987; Smith et al., 2017). Seismic waves propagate from a seismic source to the seismic receivers on the glacier surface within the seismic plane (Fig. 1). This is the vertical plane underneath the horizontal seismic profile, which runs along the surface of the glacier, and may also contain the vertical ice core axis, along which fabric information is collected. Seismic reflections occur due to sudden changes of fabric (Horgan et al., 2008, 2011; Hofstede et al., 2013) and offer the chance to obtain spatially distributed information on the COF structure in various depths of the ice column~~and laterally extended, towards a full 3d information of anisotropy in ice sheets and glaciers, which will never be feasible via the drilling of an ice core~~, the acquisition of which would be unfeasible using direct sampling via ice-coring.

The motivation of this study is to improve the interpretation of seismic data by connecting the micro- and the macro-scale using the elastic properties of ice. Early work to this end were accomplished by Bennett (1968); Bentley (1972); Blankenship and Bentley (1987) and more recent approaches include Gusmeroli et al. (2012) and Diez and Eisen (2015). Specifically, the starting point of this paper is the study by Diez and Eisen (2015), who establish a connection between the commonly ~~used~~ reported fabric parameter of second-order orientation tensor eigenvalues and the elasticity tensor describing the polycrystalline medium to calculate seismic velocities from ice-core fabric data~~(~~. (We refer to the method of Diez and Eisen (2015) as the *ev* framework~~).~~.) They illustrate the proposed calculation framework on fabric data from the polar ice core EDML (~~from the drilling EPICA~~ European Project for Ice Coring in Antarctica in Dronning Maud Land~~, Antarctica). The main objective of the here presented study is to provide a refined algorithm~~).

Our main objective is to present an improved method for the estimation of the ~~systematic deviation made by using fabric~~

~~eigenvalues for the calculation of the elasticity tensor and the derived~~ bulk elasticity tensor, and to use this to (i) evaluate the use of the *ev* framework, and (ii) demonstrate the effect of a real fabric on seismic velocities. Our study concentrates on the forward calculation of seismic velocities from the full crystal orientation distribution. The application of an inverse method will likely always require some simplification to symmetries, for which we now can quantify involved uncertainties – a required component of the covariance matrices for inverse methods.

We first present experimental measurements, theoretical basis and mathematical algorithm of our new framework (*cx*). We apply this framework to two ice cores and further investigate how fabric variability ~~on~~ at the submetre scale is reflected in theoretical seismic interval velocities. Finally, we assess the effect of asymmetrical fabric distributions on seismic velocity and explore the potential of azimuth-dependent seismic surveys.

2 Methodology

2.1 Laboratory ice fabric measurements

For our analysis of seismic velocities we use fabric data from the polar ice core EDML and the ~~Alpine~~ alpine ice core KCC. The EDML ice core was drilled as part of EPICA (European Project for Ice Coring in Antarctica) ~~until~~ between 2001 and 2006 at Kohnen Station, Antarctica, and reaches to a depth of 2774 ~~m~~ m (Oerter et al., 2009; Weikusat et al., 2017). The KCC ice core was drilled in 2013 on the ~~Alpine~~ alpine glacier Colle Gnifetti, Monte Rosa Massif, Switzerland/Italy (N 45°55.736, E 7°52.576, 4484 ~~m~~ m a.s.l.) in ~~about~~ 100 ~~m distance to~~ m distance from the ice core KCI, drilled in 2005 ~~(?)~~ (Bohleber et al., 2018) . KCC is 72 ~~m~~ m long with the firn-ice-transition at a depth of about 36 ~~m~~ m and a borehole temperature between -13.6 °C in 13 ~~m~~ m depth and -12.4 °C at the ~~bed rock~~ bedrock, measured in 2014 (pers. comm. M. Hoelzle, University of Fribourg, 2014). Both KCC and EDML were stored at ~~minimum~~ a minimum of -18 °C during transport and at -30 °C during processing.

Vertical and horizontal thin sections of the ice cores were prepared and measured ~~by means of~~ using polarised light microscopy (e.g. Wilson et al., 2003; Peternell et al., 2009) with an automatic fabric analyser from Russell-Head Instruments (models G20 and G50 in case of EDML and G50 for KCC). For each identified ice crystal in the thin section the measurement provides the orientation of the crystallographic c-axis ~~by two angles~~ $\boldsymbol{c}$ by two spherical coordinates, azimuth ϑ in the interval $(0, 2\pi)$ and colatitude φ in the interval $(0, \pi/2)$, with respect to the vertical ice-core axis that we define to coincide with the ~~z-axis~~ z-axis of the global coordinate system (Fig. 1). The c-axis is expressed in the global cartesian coordinate system $\{x, y, z\}$ as a vector ~~in spherical coordinates~~ with unit length:

$$\boldsymbol{c}(\vartheta, \varphi) = (\sin(\varphi)\cos(\vartheta), \sin(\varphi)\sin(\vartheta), \cos(\varphi)) \tag{1}$$

Figure 1 illustrates the geometric relation between the angles ϑ, φ for describing the c-axis orientations from an ice core sample and the setup of a seismic survey profile across an ice core. The incidence of a seismic wave on an ice sample is determined by the angle of incidence ψ and the azimuth angle ϑ_s of the seismic plane.

The EDML fabric data (data sets: Weikusat et al., 2013a, b, c, d) ~~is~~ are presented in detail in Weikusat et al. (2017). The total data

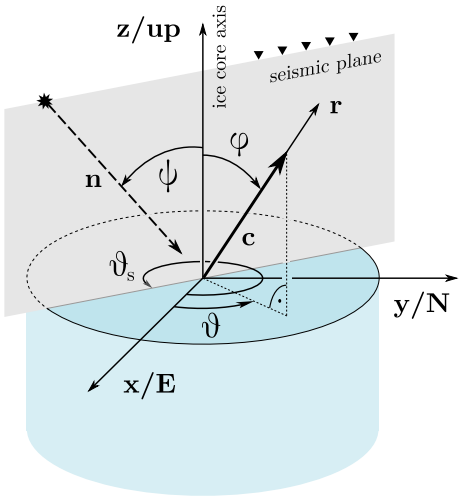

Figure 1. The global coordinate system $\{x, y, z\}$, typically corresponding to East, North and up, used for the description of a c-axis with unit length: spherical coordinates ϑ and φ specify the orientation of the c-axis. For each grain the c-axis can be expressed in its local cartesian coordinate system $\{p, q, r\}$ by $(0, 0, 1)$; p,q are not shown here. The equatorial plane ~~(dark grey)~~ corresponds to the horizontal thin section plane. The z-axis is assumed to be parallel to the ice core axis. The orientation of a hypothetical seismic plane (~~light~~ grey) is defined by the seismic azimuth angle ϑ_s, with the angle ψ of an incident seismic wave (dashed line) with unit vector normal to the plane wavefront $\boldsymbol{n}$. The star symbolises the seismic source and the triangles represent a line of seismic receivers.

set used in this study comprises 154 samples between 104 and 2563 ~~m~~ m depth with a coarse sampling interval and 40 additional vertical section samples that were measured continuously in several intervals between 2359 and 2380 m. These high resolution measurements were ~~done~~ performed with the G50 instrument. The KCC fabric data ~~(data set: Kerch et al., 2016b) consists~~ (data set: Kerch et al., 2016a, b) consist of 85 vertical thin sections ~~and covers~~ covering 11 % of the entire ice core.

Eigenvalues λ_i $(i = 1, 2, 3)$ of the second-order orientation tensor $a_{ij}^{(2)}$ are usually calculated from the c-axis distribution within a thin section sample and can be grain-, area- or volume-weighted to describe the fabric (Woodcock, 1977; Durand et al., 2006; Mainprice et al., 2011). They describe the type and strength of anisotropy in the crystal ensemble visible in the thin section (e.g. Cuffey and Paterson, 2010). Typically, different types of fabric are identified (Diez and Eisen, 2015) by the relation of the three eigenvalues with $\lambda_1 \leq \lambda_2 \leq \lambda_3$ and $\sum \lambda_i = 1$. By this classification the crystal anisotropy of the bulk can be described in a convenient way, if a unimodal distribution can be assumed, and can be associated with different deformation regimes (e.g. Weikusat et al., 2017).

2.2 Seismic wave propagation in anisotropic ice

In a glacier, the fabric anisotropy also introduces an anisotropy of the elastic properties of the material. This elastic anisotropy results in a seismic anisotropy, which means the propagation of seismic waves is influenced by the fabric anisotropy. To study this connection, theoretical velocities can be calculated if the fabric anisotropy is known.

The mathematical background for the calculation of seismic phase velocities from the elastic properties in anisotropic ice can be found in many publications (e.g. Tsvankin, 2001; Diez and Eisen, 2015). For convenience the essential concepts are shortly repeated in the following. ~~Group~~ Here we focus on phase velocities and group velocities are not ~~subject of this study and hence disregarded~~considered.

For an anisotropic elastic medium – ice behaves elastically for the propagation of seismic waves – stress and strain are linearly connected following the generalised Hooke's law:

$$\sigma_{mn} = c_{mnop}\tau_{op} \qquad \text{with} \quad m,n,o,p = 1,2,3$$

where c_{mnop} is the elasticity tensor, a fourth-order tensor which describes the medium's elastic properties. The inverse relation uses the compliance tensor s_{mnop}. Due to the symmetry of strain and stress tensor and thermodynamic considerations (Aki and Richards, 2002), the 81 unknowns of the elasticity tensor reduce to 21 independent components for general anisotropy. The elasticity tensor can then be expressed in a simplified manner, known as Voigt notation (Voigt, 1910), where pairs of indices from the fourth-order tensor are replaced by single indices. The resulting elasticity tensor in Voigt notation C_{ij} $(i,j = 1,2,3,4,5,6)$ is a symmetric second-order tensor. In the case of monocrystalline ice $\mathrm{I_h}$, the components of the elasticity tensor were measured in the laboratory by means of Brillouin spectroscopy (Gammon et al., 1983) . There are five independent components due to the hexagonal crystal symmetry. Several sets of values for the elastic moduli have been found by different authors, as summarised in Diez et al. (2015). Here, the monocrystal elasticity tensor $\mathbf{C}_\mathrm{m}$ by Gammon et al. (1983), as measured on samples of artificial ice at $-16\,^\circ\mathrm{C}$~~by means of Brillouin spectroscopy~~, is used for all calculations:

$$\mathbf{C}_\mathrm{m} = \begin{bmatrix} 13.929 & 7.082 & 5.765 & 0 & 0 & 0 \\ 7.082 & 13.929 & 5.765 & 0 & 0 & 0 \\ 5.765 & 5.765 & 15.010 & 0 & 0 & 0 \\ 0 & 0 & 0 & 3.014 & 0 & 0 \\ 0 & 0 & 0 & 0 & 3.014 & 0 \\ 0 & 0 & 0 & 0 & 0 & 3.424 \end{bmatrix} \cdot 10^9\,\mathrm{N/m^2} \tag{2}$$

To apply this description to the study of large ice sheets and glaciers, we have to consider the elastic properties of the polycrystal. The understanding of the elastic behaviour of a monocrystal can be used together with the fabric description to estimate the elastic properties of the polycrystal. Different theoretical models have been developed for the estimation of the elasticity tensor of an anisotropic polycrystal, usually making use of fabric symmetries (e.g. Nanthikesan and Sunder, 1994; Maurel et al., 2015) or by calculating orientation density functions (ODF, Mainprice et al., 2011). In this context some authors refer to the polycrystal as the "effective medium" (Maurel et al., 2015).

For the calculation of the polycrystal elastic properties from anisotropic monocrystal properties the concept of Voigt-Reuss-bounds is often used ~~. They~~ (Nanthikesan and Sunder, 1994; Bons and Cox, 1994; Helgerud et al., 2009; Vaughan et al., 2016) , and we also use this approach here. Voigt-Reuss bounds provide estimates of the upper and lower limits for the elastic moduli of the polycrystal, as was shown by Hill (1952), with the Reuss bound exceeding the Voigt bound. Nanthikesan and Sunder (1994) find that the difference of the Voigt-Reuss-bounds for the elastic moduli of polycrystalline ice does not exceed 4.2 %

and conclude that either of the bounds or an average is a good approximation.

Once the elastic properties for the polycrystal are known, the Christoffel equation provides the relationship to calculate seismic velocities. For a linearly elastic, arbitrarily anisotropic homogeneous medium the wave equation is solved by a harmonic steady-state plane wave and we obtain the Christoffel equation:

$$\begin{bmatrix} G_{11} - \rho v_{\mathrm{ph}}^2 & G_{12} & G_{13} \\ G_{21} & G_{22} - \rho v_{\mathrm{ph}}^2 & G_{23} \\ G_{31} & G_{32} & G_{33} - \rho v_{\mathrm{ph}}^2 \end{bmatrix} \begin{bmatrix} U_1 \\ U_2 \\ U_3 \end{bmatrix} = 0 \tag{3a}$$

$$\text{or} \qquad [c_{mnop} n_n n_p - \rho v_{\mathrm{ph}}^2 \delta_{mo}] U_o = 0 \tag{3b}$$

with the density ρ, the polarisation vector $\boldsymbol{U}$, the phase velocity v_{ph}, the unit vector normal to the plane wavefront $\boldsymbol{n}$, and the Kronecker delta δ_{mo}. $G_{mo} = c_{mnop} n_n n_p$ is the positive definite, thus symmetric Christoffel matrix. The vector $\boldsymbol{n}$ indicates the direction of wave propagation and depends on the angle of incidence ψ, which is measured from the vertical, and, if applicable, the azimuth angle ϑ_s between the vertical plane of incidence and the azimuthal orientation of the ice core with respect to the geocoordinates (Fig. 1):

$$\boldsymbol{n} = (\sin(\psi)\cos(\vartheta_s), \sin(\psi)\sin(\vartheta_s), \cos(\psi)) \tag{4}$$

Eq. (3) constitutes an eigenvalue problem for G_{mo}. The real and positive eigenvalues are identified with the phase velocities $v_{\mathrm{p}}, v_{\mathrm{sh}}, v_{\mathrm{sv}}$ for P-wave, SH-wave and SV-wave respectively. Different solutions are proposed, depending on the form of the elasticity tensor. The solution used in this study for an arbitrarily anisotropic medium is outlined in section 2.4.

Instead of interval velocities often the root mean square (RMS) velocity v_{rms} is considered, which gives the velocity of the homogeneous half-space equivalent to the stack of N horizontal layers (i) to this depth:

$$v_{\mathrm{rms}}(N) = \sqrt{\frac{\sum_{i=1}^{N} [v^{(i)}]^2 t_0^{(i)}}{\sum_{i=1}^{N} t_0^{(i)}}} \tag{5}$$

with the two-way ~~traveltime~~ travel time (TWT) t_0 of a seismic wave that travels vertically through a single layer with the corresponding interval velocity v. For a layered anisotropic medium a reliable depth-conversion from ~~traveltimes~~ travel times is only feasible if the RMS velocity for zero-offset can be deduced (Diez et al., 2014).

In-situ temperature and density are essential when comparing seismic velocities. However, as this study is focused on the comparison of calculation frameworks that use the same elastic moduli, a temperature correction ~~will generally not be~~ is not applied.

2.3 Recap: Eigenvalue framework

Diez and Eisen (2015) presented a framework for calculating seismic velocities from COF data in form of eigenvalues, which we briefly recapture here. In the following, this framework is referred to as ~~*ev framework*~~*ev* framework and associated variables are indicated with $^{\mathrm{ev}}$.

2.3.1 From eigenvalues to seismic interval velocities

The *ev* framework can be summarised in three steps:

1. The fabric data in the standard parameterisation of second-order orientation tensor eigenvalues are sorted into three fabric classes (cone, thick girdle, partial girdle), where each is defined by one or two opening angles χ, ϕ, symmetrical with respect to the vertical, and enveloping the c-axis distribution of a sample.

2. The opening angles characterising the fabric of each sample are used to integrate the elasticity tensor of ~~a monocrystal~~the monocrystals, Eq. (2), to obtain the elasticity tensor of the polycrystal, which exhibits an orthorhombic symmetry with respect to the vertical.

3. From the polycrystal elasticity tensor the approximative solutions to the Christoffel equation (3) for the orthorhombic case provided by Daley and Krebes (2004) are applied to obtain seismic interval phase velocities $v_{\mathrm{p}}^{\mathrm{ev}}, v_{\mathrm{sh}}^{\mathrm{ev}}, v_{\mathrm{sv}}^{\mathrm{ev}}$, which can be used for comparison with measured seismic data. Voigt calculation is used following the argument that Reuss and Voigt bounds are close enough.

2.3.2 Uncertainty of *ev* framework

The advantages of this approach are (Diez and Eisen, 2015):

- Eigenvalues are a standard parameter for expressing the strength of fabric and can be directly used for the *ev* framework without additional information about the particular measurement of thin sections from an ice core.

- By ~~restraining to~~ assuming an orthorhombic symmetry the solution to the Christoffel equation can be readily found. No information on the azimuthal orientation of the ice core (relative to any seismic measurements on a glacier) is needed, although this could be considered to improve the results in case of girdle fabric.

However, some uncertainty is inherent in the framework:

- ~~By restraining to~~ The eigenvalues of the second-order orientation tensor do not constitute a complete and unambiguous description of the fabric. Specifically, they do not provide information on preferential orientations with regard to the coordinate system. To get a rough idea about the orientation of the fabric the eigenvectors would have to be used in addition, an approach seldomly followed. Instead, the orientation of the eigenvector to the largest eigenvalue is typically assumed to correspond to the vertical, which may in fact not be the case and could introduce an unknown uncertainty.

- By assuming an orthorhombic symmetry while using opening angles to describe the c-axis distribution any information on asymmetric fabric (with respect to the vertical) is dismissed and approximation errors are introduced for more asymmetric c-axes distributions.

- ~~In fabric~~ Fabric data from ice cores ~~it can be expected~~ indicate that transitions between fabric classes ~~develop mostly~~ usually occur gradually, and ~~only in some depths sudden changes~~ sudden changes are only expected to occur due to changes in impurity content or deformation regime (Montagnat et al., 2014; Weikusat et al., 2017). However, the classification into fabric groups based on threshold values for the eigenvalues can introduce artificial discontinuities in the calculated velocity profile.

We will provide a quantitative estimate of the uncertainty of the *ev* framework in the following sections.

2.4 C-axes framework

In this study we aim to provide a quantitative estimate of the error introduced by the approximation of the *ev* framework and to assess the potential of the hitherto neglected information for future analyses. For that purpose the exact angle information of each individual c-axis is used in the following to derive the elasticity tensor $\mathbf{C}_\mathrm{p}$ of the polycrystal. Then, the phase velocities in an arbitrarily anisotropic medium are calculated. We refer to the new approach as *cx* framework. Both frameworks are summarised in Figure 2.

2.4.1 Calculating the elasticity tensor for discrete crystal ensemble

If not indicated otherwise, elasticity/compliance tensors and velocities are calculated for the effective medium, which, in this study, is typically represented by a thin section comprising a number ~~N_g of grains~~ of grains (N_g) of the order of a hundred to a thousand. Specifically, for EDML the number of grains is mostly between 100 and 650 grains per sample with the exception of some large-grained samples from the depth interval $2300-2380\,\mathrm{m}$ with less than 100 grains. For KCC the number of grains is between 155 and 1707 grains per sample and there are more than 250 grains per sample in the lowest $5\,\mathrm{m}$ of the ice core.
A data set of COF measurements from an ice core is considered that gives pairs of angles determining the c-axis of each grain $\boldsymbol{c}(\vartheta,\varphi)$ in a grain ensemble per thin section. We apply the following steps to obtain the effective elasticity tensor for a thin section sample:

1. *Transformation of the monocrystal elasticity tensor:* Considering the monocrystal elasticity tensor $\mathbf{C}_{\mathrm{m},k}$, given by Eq. (2), in the k-th grain's local coordinate frame $\{p,q,r\}$ with $\boldsymbol{c}=(0,0,1)$, a transformation (indicated by $^\mathrm{t}$) to the global coordinate frame $\{x,y,z\}$ by using the angles ~~φ,ϑ~~ ϑ,φ is necessary:

$$\mathbf{C}^\mathrm{t}_{\mathrm{m},k} = \mathbf{R}^\top_{\mathrm{C},z}\,\mathbf{R}^\top_{\mathrm{C},y}\,\mathbf{C}_{\mathrm{m},k}\,\mathbf{R}_{\mathrm{C},y}\,\mathbf{R}_{\mathrm{C},z} \tag{6}$$

with rotation matrix $\mathbf{R}_\mathrm{C}$ as given by Eq. (A3) and $\mathbf{R}^\top_\mathrm{C}$ its transpose matrix. $\mathbf{C}^\mathrm{t}_{\mathrm{m},k}$ is unlikely to have vertical transversely isotropic (VTI) symmetry, as most c-axes in a real fabric do not coincide with the z-axis, but will lie obliquely in the $\{x,y,z\}$ coordinate frame.

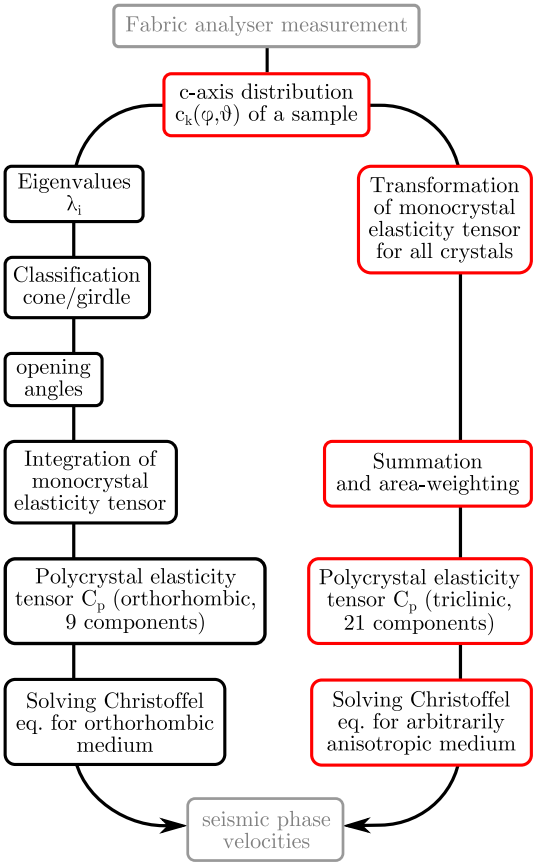

Figure 2. Flowchart to illustrate the steps for both frameworks. The work flow for the *ev* framework is framed in black boxes, starting with the eigenvalues. The work flow for the *cx* framework is framed in red and uses the c-axis distribution as input.

2. *Grain area weighting:* If grain size information is available, each transformed monocrystal elasticity tensor $\mathbf{C}^{\mathrm{t}}_{\mathrm{m},k}$ is multiplied by the grain cross-section area (A_k) fraction $f_k = A_k / \sum_k A_k$. Otherwise, it is multiplied by $1/N_{\mathrm{g}}$ for an equal contribution of all grains to the effective medium elasticity tensor.

3. *Discrete summation over the transformed monocrystal elasticity tensor for all grains to obtain the polycrystal elasticity tensor $\mathbf{C}_{\mathrm{p}}$ in the global coordinate frame:*

$$\mathbf{C}_{\mathrm{p}} = \sum_k \mathbf{C}^{\mathrm{t}}_{\mathrm{m},k} \tag{7}$$

The obtained elasticity tensor $\mathbf{C}_{\mathrm{p}}$ is very likely to have only non-zero components and describes an arbitrarily anisotropic medium.

Derivation via the compliance tensor: ~~For the aim of considering Reuss and Voigt~~ To determine the Voigt-Reuss bounds as introduced above, the polycrystal elasticity tensor is also calculated via the compliance tensor $\mathbf{S}_{\mathrm{m}}$~~, i.e.~~. To accomplish this,

the monocrystal elasticity tensor is inverted: $\mathbf{S}_\mathrm{m} = \mathbf{C}_\mathrm{m}^{-1}$. Steps 1 to 3 are then applied accordingly using Eq. (A4) to derive the compliance tensor of the polycrystal $\mathbf{S}_\mathrm{p}$, which is then again inverted to provide $\mathbf{C}_\mathrm{p}^\mathrm{R}$ ~~and indicated with~~ , where $^\mathrm{R}$ ~~(for Reuss)~~denotes Reuss.

2.4.2 Deriving seismic interval phase velocities for an arbitrarily anisotropic medium

The phase velocities $v_\mathrm{ph}(\psi, \vartheta_s)$ are obtained from the polycrystal elasticity tensor $\mathbf{C}_\mathrm{p}$ by applying the analytical solution to find the eigenvalues v_ph of the Christoffel matrix for an arbitrarily anisotropic medium, following ~~Tsvankin (2001, Appendix 1A)~~ Tsvankin (200 The algorithm is presented in Appendix B and variables associated with the *cx* framework are annotated by superscript $^\mathrm{cx}$. Thus, the velocities are calculated for any fabric, incidence angle ψ, and azimuthal orientation ϑ_s of the seismic plane.

2.4.3 Framework comparison for cone fabrics

The frameworks (*ev* and *cx*) were compared by applying them to cone fabric for all cone angles $0° \leq \phi \leq 90°$, thus excluding any effects from asymmetric fabric. We generated artificial fabric with 1000 c-axes, randomly distributed in a solid (cone) angle, in 1° steps, and calculated the respective eigenvalues. Figure 3a shows the theoretical P-wave velocity distribution $v_\mathrm{p}^{cx}(\psi, \phi)$ for all cone and incidence angles as calculated with the *cx* framework and Figure 3b gives the difference between the calculation results from both frameworks. As is to be expected the maximum velocity is found for a seismic wave at vertical incidence on a narrow single maximum fabric. The strongest velocity deviation between the frameworks is found for cone angles of approximately ~~50–60~~$50 - 60°$ at vertical incidence~~by −1.5 to 0.5~~, where the *ev* velocity exceeds the *cx* velocity by approx. 50 $\mathrm{m\,s^{-1}}$ (deviation of 1.5 %).

3 From ice core fabric to seismic velocities – case studies

We apply the *cx* framework, outlined in section 2.4, to two fabric data sets from ice cores EDML and KCC, respectively. Thus, we investigate the potential of the new framework with respect to the earlier established *ev* framework, which was already applied to fabric data from EDML (Diez et al., 2015). We use the same EDML data set (c-axis angles and grain-weighted eigenvalues), complemented by 40 additional thin sections measured more recently. The threshold ~~values~~ eigenvalues for classifying the EDML fabric within the *ev* framework are as follows: girdle fabric is given if $\lambda_2 \geq 0.2$ and $\lambda_1 \leq 0.1$, with thick girdle fabric for $0.05 < \lambda_1 \leq 0.1$ and partial girdle for $\lambda_1 \leq 0.05$; cone fabric is identified otherwise. The threshold values for classifying the KCC fabric are chosen such that only cone fabric is recognised by the algorithm, i.e. the threshold for girdle fabric is set to $\lambda_2 \geq 0.4$ and $\lambda_1 \leq 0.1$; cone fabric is identified otherwise. This is justified by the evaluation of stereographic projections of the c-axis distributions which shows that cone fabric is dominant in all KCC samples, although some tendencies towards girdle ~~can be made out~~ is observed in deeper samples, and artificial discontinuities are prevented. KCC eigenvalues are area-weighted as grain size information is available from automatic image processing. The results obtained ~~with~~ from the *cx* framework are considered to be more accurate for the purpose of comparing the frameworks in the following case studies. If not stated otherwise, all velocities are interval velocites, i.e. the seismic wave velocity within a layer, for which an elasticity

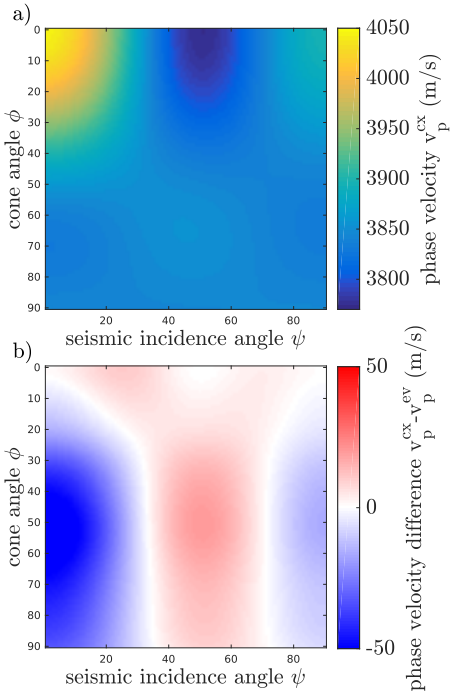

Figure 3. ~~a)~~ **a)** P-wave velocity $v_{\mathrm{p}}^{\mathrm{cx}}$ for cone fabric from randomly generated c-axes. ~~b)~~ **b)** Difference in P-wave velocity between the two frameworks for cone fabric. Blue color shows where the *ev* framework obtains higher velocities than the *cx* framework. Red shades indicate the opposite. They differ by -50 to 20 ~~$\mathrm{m\,s^{-1}}$~~ $\mathrm{m\,s^{-1}}$ (corresponding to $\leq 1.5\,\%$).

tensor is calculated based on the fabric in this layer. The velocity differences between the frameworks for the two case studies are summarised in Table 2.

3.1 Seismic interval velocity for vertical incidence

We now assess the velocity difference between the eigenvalue and the *cx* framework v_{p0} at vertical incidence of a seismic wave ~~, i.e.~~ (Figure 1, $\psi = 0°$) as indicated by subscript $_0$, with a focus on the effect of the *ev* framework fabric classification. Vertical incidence refers to the direction parallel to the ice core axis, which we assume to be normal to the glacier surface. As the seismic P-wave velocity for vertical incidence is invariant under azimuthal rotation of the seismic plane of the core, it is possible to assess the uncertainty introduced by using the eigenvalues. We mainly show results for the P-wave velocity, but included the S-wave velocity ~~for the~~ in our assessment of RMS velocities.

Vertical incidence at EDML

The evolution of the fabric of the EDML ice core becomes apparent ~~from~~ when assessing the eigenvalues (Fig. 4a) and is discussed in detail in Weikusat et al. (2017). In the following, observations are made for the comparison of the velocitites from

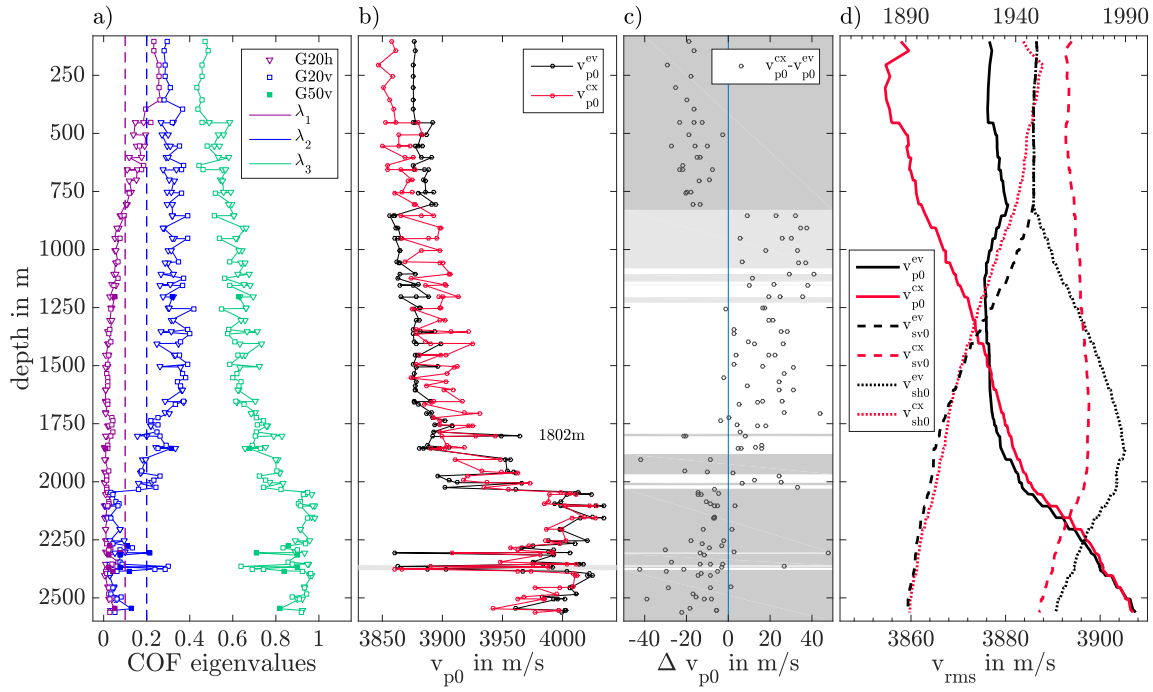

Figure 4. Comparison of zero-offset velocities calculated from EDML fabric data (without high resolution samples) via *ev* and *cx* framework. **a)** Eigenvalues (symbols and solid lines for visual assistance) and threshold values (dashed lines, *ev* framework) for girdle fabric classification. The different symbols used for eigenvalue data indicate horizontal (h, triangle) and vertical (v, square) thin sections, and the used fabric analyser model. **b)** presents the calculated interval P-wave velocities for the two frameworks. The shaded interval around 2270 ~~m~~ m indicates where high resolution measurements where taken (Fig. 5). **c)** relates the difference $\Delta v_{\mathrm{p0}} = v_{\mathrm{p0}}^{\mathrm{cx}} - v_{\mathrm{p0}}^{\mathrm{ev}}$ to the fabric classes that are indicated by shading (dark gray: cone, light gray: thick girdle, white: partial girdle). The shading extends for each data point to half the distance to the neighbouring data points. **d)** shows the seismic RMS velocities resulting from the interval velocities integrated from the surface (without taking density, temperature and firn into account); S-wave velocities refer to the upper x-axis and P-wave velocities to the lower x-axis.

the EDML ice core.

The general trend of the velocities of the two frameworks is in good agreement (Fig. 4b). However, a systematic difference can be observed (Fig. 4c): for cone fabric the P-wave velocity is overestimated by the *ev* framework, for girdle fabric the P-wave velocity is underestimated.

In the upper 1785 ~~m~~ m the velocity from the *cx* framework clearly exhibits a higher variability, as quantified by the standard deviation $s(v_{\mathrm{p0}})$ (Table 1). Below that depth, there is less variation in the velocity of the *cx* framework. The higher variability in the eigenvalue velocity below 1785 m is due to several transitions between fabric classes in the depth interval of 1800 to 2035 m; notably the prominent peak at 1802 ~~m is clearly enhanced by this.~~ m is an example of this. In the lower part of the core at 2306 ~~m~~ m a sudden weakening of the fabric anisotropy is ~~reflected~~ evident in the results of both frameworks. The velocity is, however, underestimated by the *ev* framework by 48 ~~ms^{-1} by switching~~ m s^{-1} due to a switch from cone to girdle fabric

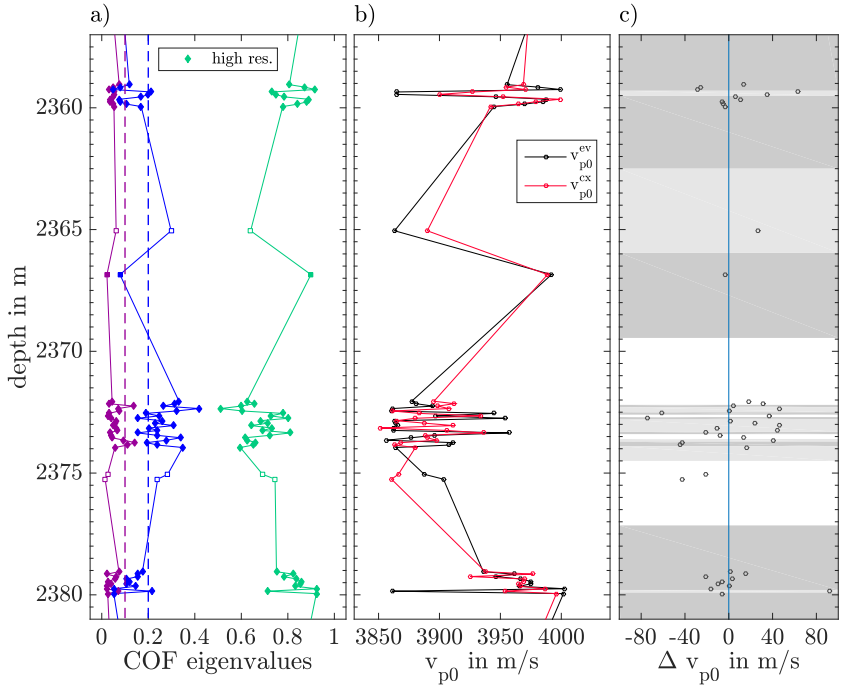

Figure 5. Comparison of P-wave velocities at vertical incidence, calculated from EDML fabric data measured in high resolution (vertical sections) between 2358 and 2380 ~~m~~ m depth with the fabric analyser G50. The same variables as in Fig. 4a-c are shown: **a)** eigenvalues, with the same symbols as defined in Fig. 4 **b)** calculated interval P-wave velocity for vertical incidence **c)** the velocity difference between frameworks and fabric classes are indicated by shading (dark gray: cone, light gray: thick girdle, white: partial girdle).

classification. RMS velocities were calculated from the interval velocities for P- and S-wave (Fig. 4d) using Eq. (5) in order to assess the cumulated effect of the velocity deviation. In the anisotropic case the zero-offset RMS velocities are needed for the depth conversion in classical reflection seismic profiles (Diez et al., 2014). For EDML, the P-wave RMS velocities $v_{\mathrm{p0,rms}}$ for the two methods converge towards the bedrock as a serendipitous result of the ~~compensation of the~~ systematic under- and overestimation described before. The S-wave RMS velocities $v_{\mathrm{s0,rms}}$ show a similar shear-wave splitting ~~(SWS)~~ of 67 ~~ms^{-1}~~ $\mathrm{m\,s}^{-1}$ and 59 ~~ms^{-1}~~ $\mathrm{m\,s}^{-1}$ at the bedrock but the *cx* velocities also show a small split in the upper 750 ~~m~~ m of the ice core, where the *ev* framework assumes a VTI fabric with no resulting shear-wave splitting.

Figure 5 is a close-up of the shaded depth in Fig. 4b and shows ~~more recent~~ high resolution measurements ~~(filled diamonds)~~ completed since Diez et al. (2015) providing ten data points per metre (filled diamonds). The new data exhibit a strong submetre-scale variability in fabric strength (Weikusat et al., 2017) which has not been regularly observed in ice-core fabric data so far (Fig. 5a). Only in recent ice core projects ~~fabric measurements have started to cover continuous intervals~~ have fabric measurements covered continuous intervals (ongoing measurements at the site of the East Greenland Ice-Core Project (EGRIP); North Gre providing new information on fabric variability. This leads to two observations: ~~1~~(i) Both frameworks produce fast changes in the interval velocity on the submetre scale and ~~2~~(ii) the fabric classification of the *ev* framework switches several times within

Table 1. Standard deviation of mean interval P-wave velocities at vertical incidence for several depth intervals of the EDML ice core.

depth in m	**std. dev.** $s(v_{\mathrm{p0}}^{\mathrm{ev}})$ **in m s^{-1}**	**std. dev.** $s(v_{\mathrm{p0}}^{\mathrm{cx}})$ **in m s^{-1}**
0 – 1785	10.9	20.3
1802 – 2035	32.8	24.1
2045 – 2563	38.5	36.4
2359 – 2360	48.3	27.9
2372 – 2374	32.3	23.0
2379 – 2380	40.3	21.3

two metres. The velocities differ by up to 90 ~~ms^{-1}~~m s^{-1}, where the *ev* framework produces more pronounced peaks than the *cx* framework. ~~This is the first time that the influence of strong fabric changes on the variation in seismic velocities over very short depth intervals is investigated.~~

Vertical incidence at KCC

~~The fabric data is discussed in detail in a forthcoming publication (in preparation).~~ We show the results of the velocity calculations for vertical incidence from the KCC fabric data in Fig. 6. The cone angle calculated from the eigenvalues varies between 10–30° for each depth interval (Fig. 6a). A detailed discussion of the fabric data is beyond the scope of this paper. The P-wave interval velocities calculated with both frameworks (Fig. 6b) increase with depth as a stronger anisotropic ~~single maximum~~ single-maximum fabric evolves and show high variability between adjacent 10 cm long samples. The difference in P-wave velocity between the two frameworks is shown in Fig. 6c. The *ev* framework overestimates the P-wave velocity ~~in~~ on average by 46 ~~ms^{-1}~~m s^{-1}. Hence, differences between the frameworks are similar for the KCC ice core as for the cone fabric regions of the EDML ice core. In the bottom layer the largest difference in P-wave velocity is -135 ~~ms^{-1}, which is~~ m s^{-1}, due to the strong single maximum ~~that is~~ inclined to the vertical. The change in c-axes velocity $\delta v_{\mathrm{p0}}^{\mathrm{cx}}$ of each 10 cm sample to the previous within a continuous measurement interval can exceed 40 ~~ms^{-1}~~ m s^{-1} (Fig. 6d). For the estimate of P-wave and S-wave RMS velocities the average velocities for each continuous measurement interval are calculated first. Then the layer boundaries are chosen such that the measured intervals are centered within the layer as indicated in Fig. 6e by the alternating shading to obtain the RMS velocities. Neither temperature nor density corrections are applied. The difference between the framework velocities at bedrock amounts to -39 ~~ms^{-1}~~ m s^{-1} for the P-wave which corresponds to an equivalent change in estimated depth of 1 %. The *cx* framework S-wave RMS velocity illustrates the shear-wave splitting which is ~~occurring, and~~ increasing with depth ~~,~~ ~~when applying the *cx* framework and which~~ and amounts to 45 ~~ms^{-1}~~ m s^{-1} (2.3 %) at bedrock.

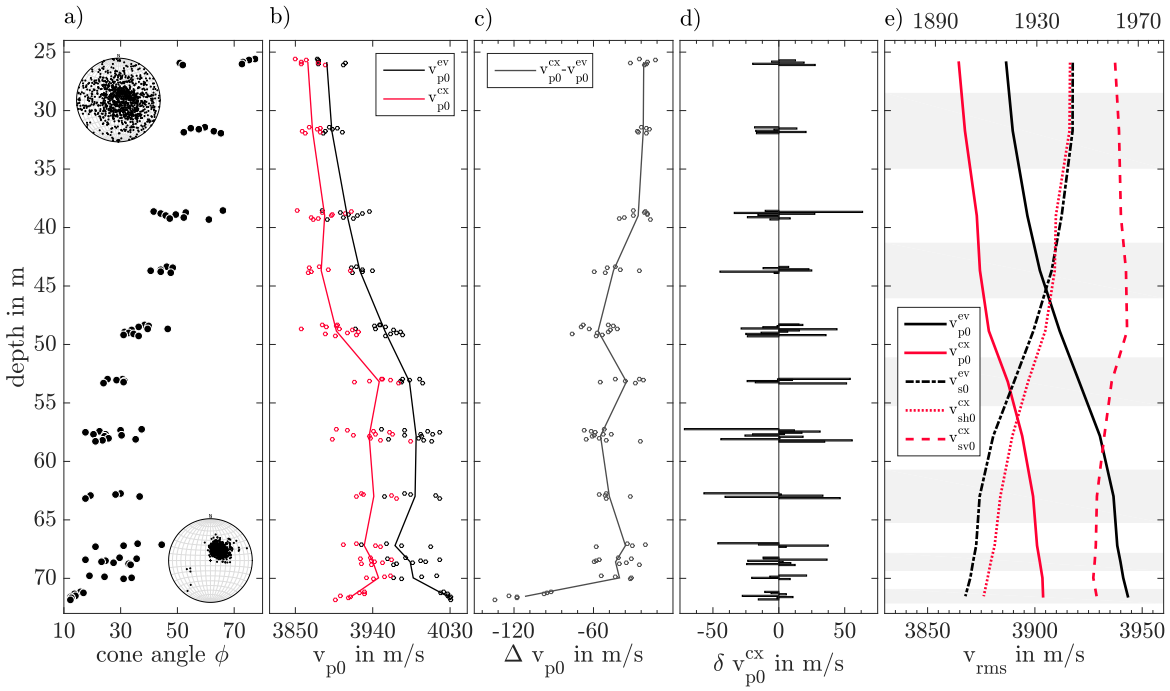

Figure 6. Comparison of zero-offset velocities calculated from KCC fabric data via ~~eigenvalue~~ *ev* and ~~c-axis~~ *cx* framework. **a)** shows cone angles derived from eigenvalues following Diez and Eisen (2015) and Schmidt diagrams illustrating the distribution of c-axes in the upper and the lower part of the core (projection of c-axes onto the horizontal ice core plane). **b)** presents the calculated P-wave velocities for the two frameworks for all thin sections (symbols) and the average velocities for each continuously sampled depth interval (lines). **c)** shows the difference $\Delta v_{p0} = v_{p0}^{cx} - v_{p0}^{ev}$ per sample and per interval average. **d)** illustrates the velocity change $\delta v_{p0}^{cx} = v_{p0}^{cx}(d_{i+1}) - v_{p0}^{cx}(d_i)$ between subsequent 10 cm sections at depths d_i. **e)** shows the RMS velocities which were calculated from the averaged velocities for layers centered around the measurement intervals (alternating shading); S-wave velocities refer to the upper x-axis and P-wave velocities to the lower x-axis.

3.2 Seismic interval velocities for non-vertical incidence

During typical seismic profile surveys the seismic wave will have an inclined angle of incidence with respect to the vertical, normal to the glacier surface. The velocities will ~~be changing in dependence of~~ vary depending on the incidence angle if the medium is anisotropic and this will affect the recorded travel times (Diez and Eisen, 2015). For a single maximum (or cone) fabric that is symmetric around the vertical this angle dependency is invariant under rotation of the seismic plane. ~~The seismic plane is the vertical x–z-plane that contains the seismic profile, which runs along the surface of the glacier in x-direction, and the ice core axis in z-direction, along which fabric information is collected (Fig. 1).~~ However, the symmetry axis of a fabric described by a set of eigenvalues could also be inclined with respect to the vertical depending on the deformation regime on site. The recorded ~~traveltimes~~ travel times will then depend on the direction of the seismic profile on the glacier surface. This, in turn, can be exploited to acquire additional information on the anisotropy. As the *cx* framework does not restrict the description

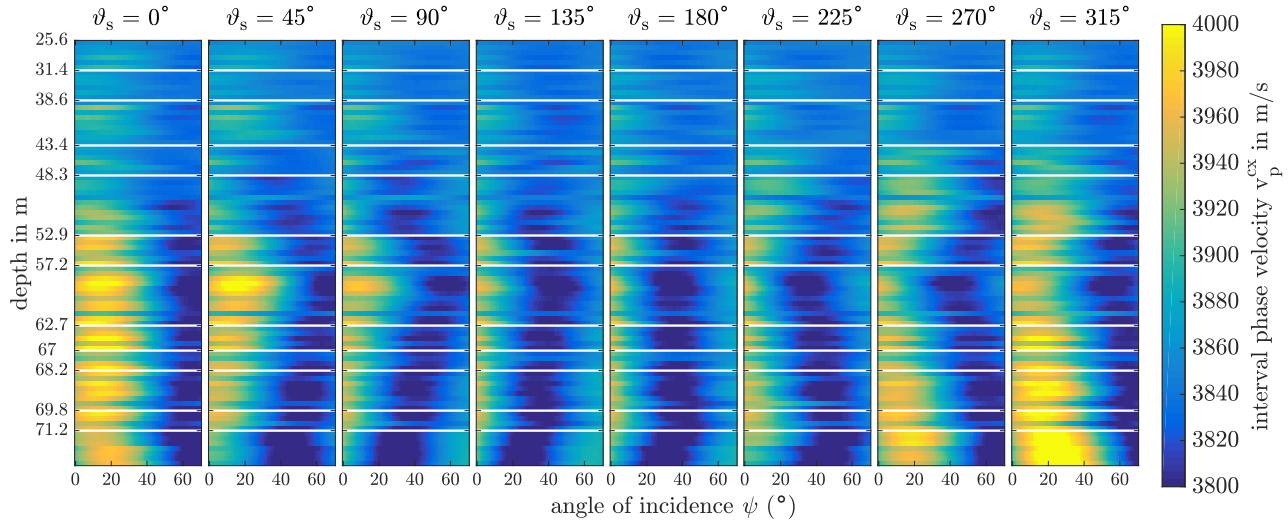

Figure 7. Seismic P-wave velocities for KCC calculated with *cx* framework for incidence angles up to 70° and eight seismic plane azimuth angles ϑ_s. The extreme values ($v_{p0} = [3779, 4030]$ ~~ms^{-1}~~m s^{-1}) lie in the saturated range of the color scale for better visual contrast. Note the breaks of the depth axis (white lines), where noted depth values refer to the top of the downward extending depth interval. The thickness of the color bands is constant for each 10 cm sample.

of the crystal anisotropy of the effective medium to a symmetry with respect to the vertical, the variation of seismic velocities under a rotating seismic plane can be studied.

In the following we assess how the seismic velocities will change when the ice core fabric data and the seismic plane of incidence are rotated with respect to each other. The zero orientation ($\vartheta_s = 0$) is not associated with any specific geographical direction. The largest uncertainty for this assessment originates in the difficulty to identify the ice core's orientation during drilling. Although it is usually tried to fit the consecutive ice core pieces during logging to maintain the correct relative orientation it is not guaranteed that there are no discontinuities. We use the term *difference* to refer to the comparison of differently calculated velocities, while *change* is used here for the azimuth-dependent observations. In this section we focus on, and begin with, the results of the ~~Alpine~~ alpine ice core KCC to demonstrate the relevance of the *cx* framework for asymmetric fabric.

Non-vertical incidence at KCC

The change of the P-wave velocity with increasing ~~phase angle~~ angle of incidence and rotated seismic plane as calculated with the azimuth sensitive *cx* framework is displayed in Fig. 7. The seismic plane is rotated around the ice core axis in steps of $\Delta\vartheta_s = 45°$. Several core pieces were presumably rotated relative to the majority of all ice core pieces during processing to optimise the aliquot cutting. The rotation was estimated and the data is corrected accordingly before applying the *cx* framework algorithm.

The influence of the asymmetry of the anisotropic fabric in the deeper part of KCC appears very clear. For some layers a

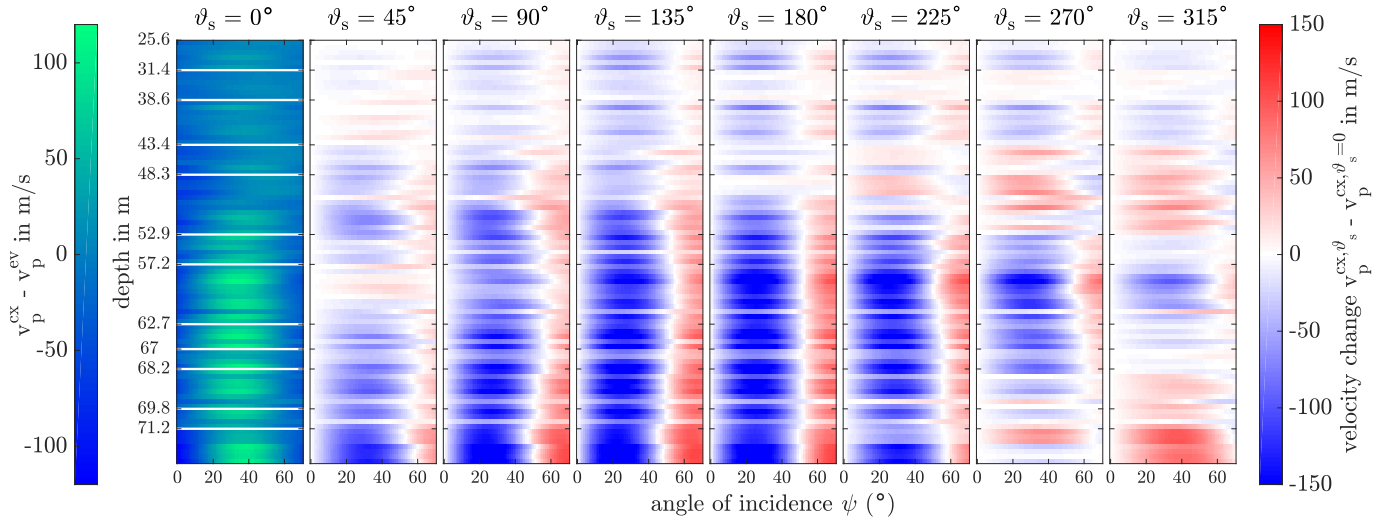

Figure 8. Left panel: Difference of KCC seismic P-wave velocity between *cx* and *ev* framework ($v_p^{cx} - v_p^{ev}$) for incidence angles up to 70°. The other panels show the change in P-wave velocity as calculated with *cx* framework for different seismic plane azimuth angles ϑ_s compared to $\vartheta_s = 0°$ ($v_p^{cx,\vartheta_s} - v_p^{cx,\vartheta_s=0}$). The extreme values ($v_p^{cx} - v_p^{ev} = [\pm 185]$ ~~ms^{-1}~~ m s^{-1} and $v_p^{cx,\vartheta_s} - v_p^{cx,\vartheta_s=0} = [-194, 109]$ ~~ms^{-1}~~ m s^{-1}) lie in the saturated range of the color scale for better visual contrast, see Table 2. Note the breaks of the depth axis where noted depth values refer to the top of the downward extending depth interval.

spread of velocities of up to 120 ~~ms^{-1}~~ m s^{-1} is observed for a given angle of incidence when considering different seismic plane azimuth angles.

The difference between the framework velocities $v_p^{cx}(\psi) - v_p^{ev}(\psi)$ is shown in Fig. 8, for $\vartheta_s = 0$. $v_p^{ev}(\psi)$ is invariant under the rotation of the seismic plane in case of cone fabric. Thus, only the *cx* velocity is changing with rotation. The change from $v_p^{cx}(\psi, \vartheta_s = 0°)$ to $v_p^{cx}(\psi, \vartheta_s)$ is shown for $\vartheta_s > 0°$. The difference in P-wave velocity when comparing the calculation frameworks reaches up to ± 190 ~~ms^{-1}~~ m s^{-1} for the bottom layer and $\pm 50 - 100$ ~~ms^{-1}~~ m s^{-1} for most depths below 48 ~~m~~ m ice depth for various incidence angles and seismic plane azimuth angles. ~~The~~

Although the slower S-waves are not routinely acquired during seismic imaging in polar environments, they provide a better resolution and are of special interest for the study of the elastic properties of ice from traditional seismic reflection profiles (Picotti et al., 2015). In particular, the splitting of the shear waves can provide unique information about the anisotropy of the medium (Anandakrishnan et al., 1994; Smith et al., 2017). In the case of the evidently asymmetric fabric of the KCC ice core we observe ~~a shear-wave~~ S-wave splitting of well above 200 ~~ms^{-1}~~ m s^{-1} in the lower half of the ice core with a maximum value of 281 ~~ms^{-1}~~ m s^{-1}. The strength of the shear-wave splitting for a particular seismic incidence angle changes when rotating the seismic plane. Figure 9 shows the difference between SV- and SH-wave velocities for non-vertical incidence (for $\vartheta_s = 0°$) and investigates how the difference between the S-wave modes changes when rotating the seismic plane. The initial difference $v_{sv}^{cx} - v_{sh}^{cx}$ at $\vartheta_s = 0°$ is low for small angles ~~but~~ except for the bottom samples. It reaches more than 200 ~~ms^{-1}~~ m s^{-1} for angles >40°. For specific azimuth angles the change in shear-wave splitting reaches about 200 ~~ms^{-1}~~ m s^{-1} for many depths

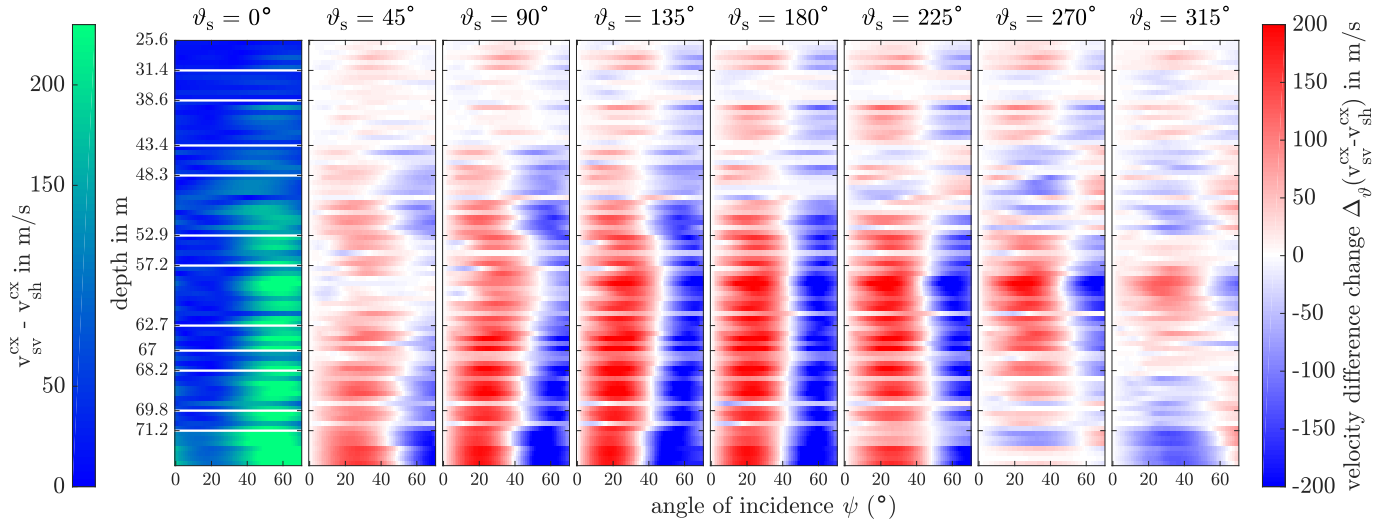

Figure 9. Top left: Difference of KCC seismic velocities between SH- and SV-wave as calculated with the *cx* framework for incidence angles up to 70°. The other seven panels give the change of the S-wave velocity difference for different seismic plane azimuth angles ϑ_s. The extreme values ($\Delta_\vartheta\,(v_{sv}^{cx} - v_{sh}^{cx}) = [-269, 238]\,\mathrm{m\,s^{-1}}$) lie in the saturated range of the color scale for better visual contrast, compare Table 2. Note the breaks of the depth axis where noted depth values refer to the top of the downward extending depth interval.

below 48 ~~m~~ m ice depth for incidence angles ~~around~~ of $10-30°$. For angles above 40° the change in S-wave velocity difference reaches -250 ~~$\mathrm{ms^{-1}}$~~ $\mathrm{m\,s^{-1}}$. The major part of this large change under seismic plane rotation is caused by the SV-wave variation.

Non-vertical incidence at EDML

~~No~~ For the EDML core, no information on the core pieces' azimuth angle relative to the ice sheet or to each other is provided. However, it is assumed that no sudden short-scale change in the flow regime can occur. Thus, abrupt offsets in girdle orientation must be caused by the unnoticed rotation of core pieces. ~~This~~ Prior to the application of the *cx* framework any misorientation needs to be corrected, or at least highlighted, to avoid misinterpretation of the results from applying the *cx* framework for seismic velocity calculation considering non-vertical ~~phase~~ incidence angles. For the EDML data set the orientation of several single thin sections was corrected according to the girdle orientation of the neighbouring thin sections. ~~A~~ For instance, a sharp change of girdle direction of about 45° in 1705 ~~m~~ m (Weikusat et al., 2017) could not be corrected and has to be kept in mind when looking at the velocity calculation results for non-vertical incidences.

As the *ev* framework does not aim to include the orientation of the girdle, the velocity in girdle fabric is considered as invariant under the rotation as well. We therefore only assess the change in P-wave velocity v_p^{cx} as calculated with the *cx* framework (Fig. 10). The respective figures for S-wave velocities can be found in Kerch (2016). The highest seismic P-wave velocities ($\sim$4028 ~~$\mathrm{ms^{-1}}$~~ $\mathrm{m\,s^{-1}}$) calculated with the *cx* framework for non-vertical incidence are found deeper than 2000 m, where the

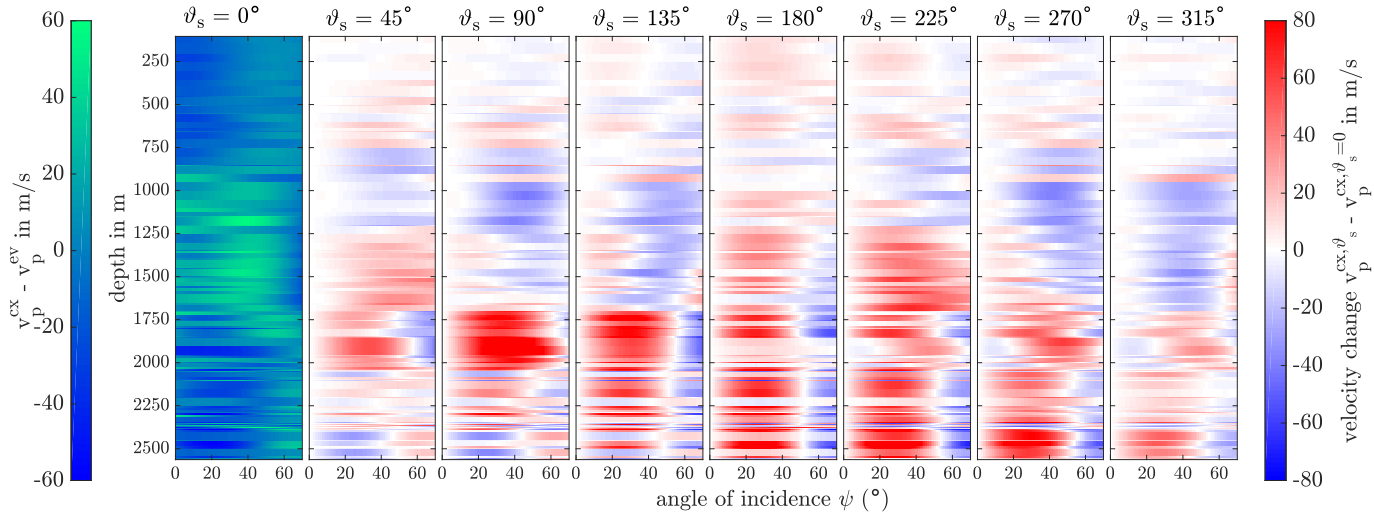

Figure 10. Left panel: Difference of EDML seismic P-wave velocity between *cx* and *ev* framework ($v_p^{cx} - v_p^{ev}$) for incidence angles up to 70°. The other panels show the change in P-wave velocity as calculated with *cx* framework for different seismic plane azimuth angles ϑ_s compared to $\vartheta_s = 0°$ ($v_p^{cx,\vartheta_s} - v_p^{cx,\vartheta_s=0}$). The extreme values ($v_p^{cx,\vartheta_s} - v_p^{cx,\vartheta_s=0} = [-97, 150]\,\mathrm{m\,s^{-1}}$) lie in the saturated range of the color scale for better visual contrast, see Table 2. Where the core orientation is insufficiently known and corrected with respect to neighbouring core pieces, vertical variation in velocity in dependence of the incidence angle may not be a true variation.

fabric anisotropy is strong, for ~~phase~~ incidence angles below 20°. Seismic P-wave velocities are underestimated by the *ev* framework by max. 131 ~~ms^{-1}~~ $\mathrm{m\,s^{-1}}$ and overestimated by max. 84 ~~ms^{-1}~~ $\mathrm{m\,s^{-1}}$. The difference is only small ($\pm$ 20 ~~ms^{-1}~~ $\mathrm{m\,s^{-1}}$) for cone fabric in the upper part (0 – 800 m). The highest change is apparent for the lower part of the girdle fabric, below the earlier mentioned sudden rotation of the dominant azimuth direction, and for cone fabric in the deep part of the core. There, the change in interval velocity can exceed 100 ~~ms^{-1}~~ $\mathrm{m\,s^{-1}}$ for some seismic azimuth planes as compared to the defined 0°-plane.

4 Discussion

~~The velocity differences between the frameworks for the two case studies are summarised in Table 2.~~

Evaluation of the *cx* framework

The *cx* framework provides a refined approach for the use of fabric information to obtain seismic velocities in ice. By ~~omitting the eigenvalues~~ including all the c-axis observations, instead of using eigenvalue representation, we keep information that is lost with the *ev* framework and we avoid the approximation to the true c-axis distribution by deriving opening angles. We average on the crystal scale to obtain the full elasticity tensor for the polycrystalline ice. This is, to our knowledge, the first time this approach has been applied to actual ice-core fabric data. Recent work from Vaughan et al. (2017) presents P-wave velocities from cryo-EBSD data on artificial ice using the MTEX toolbox (Mainprice et al., 2011).

By using the fabric data from thin sections we acknowledge the uncertainty which arises from sampling with a relatively small sample size. We use less than 1 % of the ice core EDML and 11 % of the ice KCC to infer the fabric development in the ice cores. There is currently no comprehensive data available to investigate the sampling effect on real ice. As we are concerned with the comparison of theoretical seismic velocities calculated from the same fabric data, we assume that the sampling uncertainty can be neglected. For the comparison with measured seismic data the uncertainty needs to be considered, ~~as well as the~~ and appropriate density and temperature ~~correction~~corrections are required.

The observed variation in eigenvalues in the EDML ice core (Fig. 4a) can partly be attributed to a systematic deviation between horizontal and vertical thin sections which is a bias produced by the older fabric analyser model G20 (Weikusat et al., 2017). Both the short-scale variation in the high resolution intervals in the EDML ice core and in the KCC ice core are not affected by the instrument bias. The *cx* framework ~~seems to reflect~~ propagates this systematic variability ~~stronger than~~ more that the *ev* framework, with a higher standard deviation for the EDML depth interval $0 - 1785$ ~~m~~ m (Table 1), illustrating the higher sensitivity to small fabric differences. The measurement of c-axes from thin sections with the instrument and the subsequent automatic image processing, which provides the c-axis angles as an average per grain, contribute to a smaller extent to the overall uncertainty at a level which is difficult to quantify. However, the processing routine (Eichler, 2013) has proven to provide robust results with respect to minor changes in the procedure and algorithm.

The currently employed algorithms for the calculation of seismic velocities in ice polycrystals on the crystal scale (including this study) do not consider any possible effects on the grain boundaries. For laboratory measurements the difference in stress on a polycrystalline ice sample as compared with in-situ conditions can affect the degree to which grains are bonding and, thus, the elasticity (Helgerud et al., 2009). Processes like grain boundary sliding are currently explored in the context of deformation mechanism on the micro-scale (pers. comm. E.-J. Kuiper, Univ. of Utrecht, 2017) but can also influence the elastic behaviour of ice (Elvin, 1996). These issues should be addressed for future applications employing ultrasonic methods for the estimation of elastic properties of ice.

The lack of knowledge about the dispersion of seismic waves in ice introduces an unknown uncertainty to the calculation based on a monocrystal elasticity tensor that was measured in the laboratory by means of ultrasonic sounding. Again, for the application of ultrasonic methods, which operate in the same frequency range, this uncertainty can be neglected. The connection of fabric and seismic velocities on the crystal scale we present here complements this advancing field of study.

We have shown in section 2.4.3 that the *ev* and *cx* frameworks differ slightly in the case of vertically symmetric cone fabric for vertical incidence and large cone angles. This type of fabric can commonly be expected in the shallower depth of any glacier where vertical compression is dominant. We conclude that the observed deviation in the vertical P-wave velocity profile (EDML) between the *ev* and the *cx* velocity for cone fabric could partly be attributed to this inherent difference between the frameworks.

In the case of asymmetric c-axis distributions, as observed in the KCC ice core, we obtain large differences between the interval velocities of the two frameworks, resulting in a detectable difference between the RMS velocities at the bedrock which is relevant for the depth conversion. We can confirm the assessment of Voigt-Reuss bounds to lie below 1 % (for P-wave) in our study.

~~A main~~ An advantage of the *cx* framework is the ~~dispensation with~~ lack of a need for the fabric classification, thus eliminating artificial discontinuities. In synthetic seismograms derived from the modelled velocities, such artefacts could result in artificial reflectors and, thus, lead to false interpretations. The example of high resolution sampling in the EDML ice core demonstrates the importance of this advance, allowing us to separate the true high variability in seismic velocities from the artificially enhanced variability. This finding could, however, be used to tune the threshold values for the fabric classification in the *ev* framework.

Potentially, our framework can be used in principle for the development of inverse methods to derive the fabric distribution from seismic velocities. Following experience from other fields of active seismology, this would, first, most likely require comprehensive data sets suitable for full-waveform inversion not yet available for glaciological applications, and, second, some simplifying assumptions on the distribution of crystal fabric, e.g. in terms of considered symmetries. The framework we presented allows to quantify the potential effect of simplifying assumptions and could help to more accurately specify covariance matrices, thus enabling the quantification of uncertainties coming along with the results produced by application of an inverse method.

Azimuth-sensitive seismic velocities

The *cx* framework we developed and employed in this study takes into account the asymmetry of anisotropic fabric, with respect to the vertical. This is especially relevant for glacial environments with a complex flow pattern, for example in sloping mountain glaciers, fast-flowing polar outlet glaciers ~~(?)~~ (Hofstede et al., 2018) and ice streams (Smith et al., 2017). For such sites the approximation of the fabric by opening angles centered around the vertical can deviate much more from the reality than for sites that are located in the vicinity of an ice divide. It becomes evident from the presented KCC case study that the azimuthal change of the fabric and the resulting velocities are not negligible. On the contrary, the velocities calculated with the *cx* framework for non-vertical incidence angles from an arbitrary seismic azimuth can change strongly for both P- and ~~S-wave~~ S-waves and the associated shear-wave splitting. If the velocity depth profile changes continuously, as is illustrated in Fig. 7, 8 and 9, this should, in principle, be resolved in seismic surface profile data from different seismic azimuth directions, providing information about the (asymmetric) crystal anisotropy evolution with depth.

A requirement of the *cx* framework is the dependency on accurate core orientation information, i.e. the orientation of the fabric distribution in the equatorial plane has to be known for the consecutive fabric samples. To ~~this~~ date, the ~~oriented drilling~~ retrieval of ice cores with known azimuth remains a challenge. Hence, the uncertainty ~~for~~ in the calculation of seismic velocities is much larger in the vertical direction than under azimuthal rotation. On the other hand, analysing seismic data with azimuthal resolution around an ice core drilling site could provide the information to improve the reconstruction of the core orientation. The appearance of a non-symmetric fabric might also be induced by inclined drilling. Ideally, to be able to link calculated and measured seismic velocities a possible inclination of the ice core with respect to the vertical and to the horizontal seismic profile should be considered.

Rapid velocity changes over ~~small~~ short vertical distances

We use COF measurements on a submetre scale for our analysis of seismic velocities. The results suggest the existence of closely spaced reflective surfaces for elastic seismic waves (and also radar waves). The relevance of the presented analysis for real seismic data is based on the major assumption of a laterally extended and coherent fabric layering on the scale of the first Fresnel zone (Drews et al., 2012). Although fabric layering is regularly observed in the KCC ice core and also in the continuously sampled depth intervals in EDML, it is still unclear how representative these short-scale variations are for both the close vicinity and a larger region in a glacier. However, evidence has been presented for abrupt COF changes as a frequent cause of seismic reflectivity (Horgan et al., 2011). Other studies do not observe such a high reflectivity due to COF but identify a high degree of gradually evolving fabric anisotropy (Picotti et al., 2015) or single strong reflections associated with transitions in fabric classes, e.g. from cone to girdle (Diez et al., 2015). The coherence of thin layers with distinct fabric will largely depend on the unresolved question of how they evolve exactly. If the short-scale fabric stratigraphy is largely governed by local conditions and ~~heterogenous~~ heterogeneous small-scale deformation, possibly resulting in "layer roughness" (Drews et al., 2009), no coherent structure is to be expected (Diez et al., 2015). In this case, it should be challenged, how representative the elastic properties derived from thin sections are, and the question arises, how ~~non-coherent~~ incoherent short-scale fabric changes alter the rheological properties of the bulk. It can be hypothesised that under the increasing influence of large-scale shear deformation in the deeper regions of the glacier coherent fabric layers might develop. Accordingly, more seismic reflectivity should be expected in depth and from more dynamic settings, as proposed by Horgan et al. (2011). Eisen et al. (2007) show that transitions in COF in the deep ice can be followed with radio-echo sounding over longer horizontal distances of several kilometres. However, variations in seismic velocity on short vertical scales cannot be resolved with conventional surface-based seismic techniques with large wavelengths of the order of 10 m, depending on the source of the seismic waves and the sounding depth. Still, Hofstede et al. (2013) obtain numerous laterally continous reflections at Halvfarryggen, Antarctica. They suggest that closely spaced layers ("stacks") of varying fabric, possibly as ~~has~~ have been observed in this study, are the major cause for the reflections.

Far more fabric data than is currently sampled in ice core studies, is required to pursue this hypothesis in the future. To this end, ultrasonic methods can be applied in ice core boreholes (Bentley, 1972; Gusmeroli et al., 2012) to infer crystal-orientation fabric in situ. Although the interpretation of these data is not straightforward (Maurel et al., 2015), it is currently the only technique that is capable of a continuous fabric measurement. However, a sonic pulse samples the volume around the borehole ($\sim 2\,m^3$, Gusmeroli et al., 2012), which means the method is not azimuth-sensitive. While it cannot provide the two-dimensional microstructure nor exact and highly resolved fabric information, it can help to bridge the gap between laboratory-based interval fabric measurements and large-scale seismic data.~~Following the perceptions of the present~~ Following the findings of our study we recommend for seismic data acquisition in the field to (1) consider polarimetric survey setups (with two or even more crosslines) with both reflection and wideangle measurements, and to (2) focus on accurate travel time recordings at high source frequencies. This should be supported by 3-component vertical seismic profiling where boreholes are available. Also, S-waves should be acquired as they provide useful information on crystal anisotropy due to

shear-wave splitting. On the crystal scale, we suggest to include the investigation of the possible influence of variations in grain size for the ~~seismic~~ elastic wave propagation in polycrystalline ice, which is currently not considered for theoretical calculations, to complement recent work on the temperature dependency of elastic properties (Vaughan et al., 2016). Ongoing microstructure studies on both ~~Alpine~~ alpine and polar ice provide indications of considerable vertical short-scale variability in grain topology. Recent laser ultrasound measurements on ice have provided first high-resolution data (Mikesell et al., 2017) and promise further advances towards understanding and efficiently measuring the elastic properties of polycrystalline ice on the crystal scale.

5 Conclusions and Outlook

The presented *cx* framework contributes to the understanding of the propagation of seismic velocities in glacial ice by deriving bulk elastic properties on the crystal scale. Based on anisotropic fabric from two ice cores, we showed that the fabric classification scheme in the *ev* framework can mask the true velocity variability by producing artificially enhanced peaks in the velocity profile. By applying the *cx* framework we extract the velocity variability that is caused by the actual fabric variability. The velocity difference between the *cx* and *ev* frameworks is larger for the ~~Alpine~~ alpine than for the polar core. This suggests that the *ev* framework provides a good enough approximation for the polar site, situated on an ice divide, for the current degree of seismic resolution and interpretation of physical properties, not considering the artificial discontinuities, but is not adequate for the ~~Alpine~~ alpine site.

We found that the azimuthal change in P-wave velocity and shear-wave splitting can be as large as $\sim 200\,$~~ms^{-1}~~m s^{-1}. We conclude that the possibility of an azimuthal asymmetry of the fabric distribution should be considered when planning seismic surveys (e.g. polarimetric profiles around a drilling site) as well as for the calculation of seismic velocities from fabric data. This also offers an opportunity to further constrain azimuthal ice-core orientation.

The results of our study demonstrate for the first time that a short-scale variability in anisotropic fabric as observed in these polar and ~~Alpine~~ alpine ice cores causes a corresponding high short-scale variability in seismic interval velocities. Current laboratory fabric measurements from an ice core drilled on an ice stream also show early indications of a high fabric variability and unexpected fabric types (pers. comm. J. Eichler, 2017), offering an ideal target for extending this study to an environment with another deformation regime. Based on the presented evidence in this study the next steps should include the investigation of how a succession of short-scale fabric layers could induce englacial reflections as has been reported and hypothesised in earlier studies (Horgan et al., 2011; Hofstede et al., 2013).

As conventional surface-based seismic surveys are not likely to resolve ~~these~~ this short-scale ~~variabilities~~variability, ultrasonic techniques for borehole and laboratory studies could be the solution to both issues of lost core orientation and low resolution. For this emerging field of applications, we offer further insight into what to expect from crystal-orientation fabric anisotropy in ice. Equally, our results can provide context for data collected with frozen-in seismometers in boreholes, where evidence for shear-wave splitting on non-vertical ray paths was found ~~(?)~~ (pers. comm. David Prior, 2018). Lastly, we want to highlight that while the depth scale of the KCC ice core differs from that of the EDML ice core by a factor of 1/35, the presented case

study is another example (Eisen et al., 2003; Diez et al., 2014) of the importance of mid-latitude high-altitude glaciers as in-situ laboratories to study fundamental processes in glaciers.

Data availability. The fabric and eigenvalue data sets for the ice cores KCC (Kerch et al., 2016a, b) and EDML (Weikusat et al., 2013a, b, c, d) are published in the open-access database PANGAEA® and available upon request.

Appendix A: Tensor transformation

A fourth-order tensor rotation is expressed as:

$$c^{\mathrm{rot}}_{mnop} = R_{mi}R_{nj}R_{ok}R_{pl}c_{ijkl}$$

$$\text{or} \quad \mathbf{C}^{\mathrm{rot}} = \mathbf{R}\cdot\mathbf{R}\cdot\mathbf{C}\cdot\mathbf{R}^{\top}\cdot\mathbf{R}^{\top}$$

The general rotation matrix in three dimensions is given by the cosines between the axes of local $\{p,q,r\}$ and global $\{x,y,z\}$ coordinate frame:

$$\mathbf{R} = \begin{pmatrix} \cos(x,p) & \cos(x,q) & \cos(x,r) \\ \cos(y,p) & \cos(y,q) & \cos(y,r) \\ \cos(z,p) & \cos(z,q) & \cos(z,r) \end{pmatrix} = \begin{pmatrix} l_1 & l_2 & l_3 \\ m_1 & m_2 & m_3 \\ n_1 & n_2 & n_3 \end{pmatrix} \tag{A1}$$

For a coordinate transformation of the monocrystal elasticity tensor $\mathbf{C}_{\mathrm{m}}$ from crystal to global frame two basic rotations are needed, one around the y-axis given by the colatitude angle φ and another around the z-axis with azimuth ϑ:

$$\mathbf{R}_y = \begin{pmatrix} \cos(\varphi) & 0 & \sin(\varphi) \\ 0 & 1 & 0 \\ -\sin(\varphi) & 0 & \cos(\varphi) \end{pmatrix}, \quad \mathbf{R}_z = \begin{pmatrix} \cos(\vartheta) & -\sin(\vartheta) & 0 \\ \sin(\vartheta) & \cos(\vartheta) & 0 \\ 0 & 0 & 1 \end{pmatrix} \tag{A2}$$

It is possible to express both rotations in a single rotation matrix (as done by Maurel et al., 2015, section 3).

By using Voigt notation, which mathematically implies a change of base, the rotation matrix $\mathbf{R}_{\mathrm{C}}$ for the elasticity tensor is constructed following Sunder and Wu (1990, see appendix) using the parameterisation in Eq. (A1) and Eq. (A2) for the respective rotation:

$$\mathbf{R}_{\mathrm{C}} = \begin{pmatrix} l_1^2 & m_1^2 & n_1^2 & m_1n_1 & n_1l_1 & l_1m_1 \\ l_2^2 & m_2^2 & n_2^2 & m_2n_2 & n_2l_2 & l_2m_2 \\ l_3^2 & m_3^2 & n_3^2 & m_3n_3 & n_3l_3 & l_3m_3 \\ 2l_2l_3 & 2m_2m_3 & 2n_2n_3 & m_2n_3+m_3n_2 & n_2l_3+n_3l_2 & l_2m_3+l_3m_2 \\ 2l_3l_1 & 2m_3m_1 & 2n_3n_1 & m_3n_1+m_1n_3 & n_3l_1+n_1l_3 & l_3m_1+l_1m_3 \\ 2l_1l_2 & 2m_1m_2 & 2n_1n_2 & m_1n_2+m_2n_1 & n_1l_2+n_2l_1 & l_1m_2+l_2m_1 \end{pmatrix} \tag{A3}$$

The rotation matrix $\mathbf{R}_{\mathrm{S}}$ for the compliance tensor is given by:

$$\mathbf{R}_{\mathrm{S}} = \begin{pmatrix} l_1^2 & m_1^2 & n_1^2 & 2m_1n_1 & 2n_1l_1 & 2l_1m_1 \\ l_2^2 & m_2^2 & n_2^2 & 2m_2n_2 & 2n_2l_2 & 2l_2m_2 \\ l_3^2 & m_3^2 & n_3^2 & 2m_3n_3 & 2n_3l_3 & 2l_3m_3 \\ l_2l_3 & m_2m_3 & n_2n_3 & m_2n_3+m_3n_2 & n_2l_3+n_3l_2 & l_2m_3+l_3m_2 \\ l_3l_1 & m_3m_1 & n_3n_1 & m_3n_1+m_1n_3 & n_3l_1+n_1l_3 & l_3m_1+l_1m_3 \\ l_1l_2 & m_1m_2 & n_1n_2 & m_1n_2+m_2n_1 & n_1l_2+n_2l_1 & l_1m_2+l_2m_1 \end{pmatrix} \tag{A4}$$

The expressions for $\mathbf{R}_{\mathrm{C}}$ and $\mathbf{R}_{\mathrm{S}}$ as given in Diez and Eisen (2015, Eq. (A.6) and (A.7)) are reversed by mistake.

Appendix B: Analytical solution to finding eigenvalues to the elasticity tensor

From the characteristic polynomial of Eq. (3) a cubic equation can be derived with the substitution $\rho v_{\mathrm{ph}}^2 \rightarrow y - a/3$:

$$\det[G_{mo} - \rho v_{\mathrm{ph}}^2 \delta_{mo}] = y^3 + dy + q = 0$$

where the coefficients d and q follow from combinations a, b, c given by the components of the Christoffel matrix G_{mo}:

$$\begin{aligned} a &= -(G_{11}+G_{22}+G_{33}) \\ b &= G_{11}G_{22}+G_{11}G_{33}+G_{22}G_{33}-G_{12}^2-G_{13}^2-G_{23}^2 \\ c &= G_{11}G_{23}^2+G_{22}G_{13}^2+G_{33}G_{12}^2-G_{11}G_{22}G_{33} \\ &\quad -2G_{12}G_{13}G_{23} \\ d &= b-a^2/3 \\ q &= 2a^3/27-ab/3+c \end{aligned}$$

For $k = 0, 1, 2$ the velocities $v_{\mathrm{p}}^{\mathrm{cx}}$, $v_{\mathrm{sh}}^{\mathrm{cx}}$, $v_{\mathrm{sv}}^{\mathrm{cx}}$ are found from

$$v_{\mathrm{ph}}(k) = \left\{ \left[\left(\frac{2}{\sqrt{3}} \sqrt{-d} \cos\left[\frac{1}{3} \left(\arccos\left(-\frac{q}{2\sqrt{(-d/3)^3}} \right) + 2\pi k \right) \right] \right) - \frac{a}{3} \right] \rho^{-1} \right\}^{1/2} \tag{B1}$$

and are real under the conditions:

$$\frac{q^2}{4} + \frac{d^3}{27} \leq 0 \quad \text{and} \quad 0 \leq \arccos\left(-\frac{q}{2\sqrt{(-d/3)^3}} \right) \leq \pi \tag{B2}$$

The algorithm is implemented in MATLAB® for this study.

Author contributions. The study was initiated and supervised by O.E. The fabric data was collected and analysed by I.W. (EDML) and J.K. (KCC), supervised by I.W. Calculations were conducted by J.K., supported by discussions with A.D. The paper was written by J.K., with comments and suggestions for improvement from all co-authors.

Competing interests. The authors declare that there are no competing interests.

Acknowledgements. We would like to thank the KCC drilling team with collegues from the Institute of Environmental Physics (Heidelberg University, Germany), the Climate Change Institute (University of Maine, USA) and the Institute for Climate and Environmental Physics (University of Bern, Switzerland). Many thanks to D.J. for suggestions for the improvement of the manuscript. J.K. was funded by the Studienstiftung des deutschen Volkes and supported by HGF grant no. VH-NG-803 to I.W. We gratefully acknowledge M. Montagnat and H. Horgan for their helpful comments to improve the manuscript and M. Schneebeli for editing of this manuscript.

References

Aki, K. and Richards, P. G.: Quantitative seismology, 2002.

Anandakrishnan, S., Fltzpatrick, J., Alley, R., Gow, A., and Meese, D.: Shear-wave detection of asymmetric c-axis fabrics in the GISP2 ice core, Greenland, J. Glaciol., 40, 491–496, doi:10.3198/1994JoG40-136-491-496, 1994.

Bennett, H. F.: An investigation into velocity anisotropy through measurements of ultrasonica wave velocities in snow and ice cores from Greenland and Antarctica, Ph.D. thesis, University of Wisconsin-Madison, 1968.

Bentley, C. R.: Seismic-wave velocities in anisotropic ice: A comparison of measured and calculated values in and around the deep drill hole at Byrd Station, Antarctica, J. Geophys. Res., 77, 4406–4420, 1972.

Blankenship, D. D. and Bentley, C. R.: The crystalline fabric of polar ice sheets inferred from seismic anisotropy, IAHS Publ., 170, 17–28, 1987.

Bohleber, P., Erhardt, T., Spaulding, N., Hoffmann, H., Fischer, H., and Mayewski, P.: Temperature and mineral dust variability recorded in two low-accumulation Alpine ice cores over the last millennium, Clim. Past, 14, 21–37, doi:10.5194/cp-14-21-2018, 2018.

Bons, P. D. and Cox, S. J.: Analogue experiments and numerical modelling on the relation between microgeometry and flow properties of polyphase materials, Mater. Sci. Eng., 175, 237–245, doi:10.1016/0921-5093(94)91063-4, 1994.

Cuffey, K. and Paterson, W.: The Physics of Glaciers, Academic Press, 4th edition edn., 2010.

Daley, P. and Krebes, E.: Alternative linearized expressions for qP, qS1 and qS2 phase velocities in a weakly anisotropic orthorhombic medium, CREWES Annual Report, 21, 2004.

Diez, A. and Eisen, O.: Seismic wave propagation in anisotropic ice – Part 1: Elasticity tensor and derived quantities from ice-core properties, The Cryosphere, 9, 367–384, doi:10.5194/tc-9-367-2015, 2015.

Diez, A., Eisen, O., Weikusat, I., Eichler, J., Hofstede, C., Bohleber, P., Bohlen, T., and Polom, U.: Influence of ice crystal anisotropy on seismic velocity analysis, Ann. Glaciol., 55, 97–106, doi:10.3189/2014AoG67A002, 2014.

Diez, A., Eisen, O., Hofstede, C., Lambrecht, A., Mayer, C., Miller, H., Steinhage, D., Binder, T., and Weikusat, I.: Seismic wave propagation in anisotropic ice – Part 2: Effects of crystal anisotropy in geophysical data, The Cryosphere, 9, 385–398, doi:10.5194/tc-9-385-2015, 2015.

Drews, R., Eisen, O., Weikusat, I., Kipfstuhl, S., Lambrecht, A., Steinhage, D., Wilhelms, F., and Miller, H.: Layer disturbances and the radio-echo free zone in ice sheets, The Cryosphere, 3, 195–203, 2009.

Drews, R., Eisen, O., Steinhage, D., Weikusat, I., Kipfstuhl, S., and Wilhelms, F.: Potential mechanisms for anisotropy in ice-penetrating radar data, J. Glaciol., 58, 613–624, doi:10.3189/2012JoG11J114, 2012.

Durand, G., Weiss, J., Lipenkov, V., Barnola, J. M., Krinner, G., Parrenin, F., Delmonte, B., Ritz, C., Duval, P., Röthlisberger, R., and Bigler, M.: Effect of impurities on grain growth in cold ice sheets, J. Geophys. Res., 111, 1–18, doi:10.1029/2005JF000320, 2006.

Eichler, J.: C-Axis analysis of the NEEM ice core – An approach based on digital image processing, Diploma thesis, Freie Universität Berlin and Alfred-Wegener-Institut Bremerhaven, 2013.

Eichler, J., Weikusat, I., and Kipfstuhl, S.: C-axis fabric analysis of ice samples collected from the NEEM ice core, doi:10.1594/PANGAEA.838063, 2013.

Eisen, O., Nixdorf, U., Keck, L., and Wagenbach, D.: Alpine ice cores and ground penetrating radar: combined investigations for glaciological and climatic interpretations of a cold Alpine ice body, Tellus B, 55, 1007–1017, 2003.

Eisen, O., Hamann, I., Kipfstuhl, S., Steinhage, D., and Wilhelms, F.: Direct evidence for continuous radar reflector originating from changes in crystal-orientation fabric, The Cryosphere, 1, 1–10, doi:10.5194/tc-1-1-2007, 2007.

Elvin, A. A.: Number of grains required to homogenize elastic properties of polycrystalline ice, Mechanics of Materials, 22, 51–64, doi:10.1016/0167-6636(95)00024-0, 1996.

Faria, S. H., Weikusat, I., and Azuma, N.: The microstructure of polar ice. Part II: State of the art, J. Struct. Geol., 61, 21–49, doi:10.1016/j.jsg.2013.11.003, microdynamics of Ice, 2014.

Gammon, P., Kiefte, H., Clouter, M., and Denner, W.: Elastic constants of artificial and natural ice samples by Brillouin spectroscopy, J. Glaciol., 29, 433–460, 1983.

Gusmeroli, A., Pettit, E. C., Kennedy, J. H., and Ritz, C.: The crystal fabric of ice from full-waveform borehole sonic logging, J. Geophys. Res., 117, 1–13, doi:10.1029/2012JF002343, 2012.

Helgerud, M. B., Waite, W. F., Kirby, S. H., and Nur, A.: Elastic wave speeds and moduli in polycrystalline ice Ih, sI methane hydrate, and sII methane-ethane hydrate, J. Geophys. Res., 114, doi:10.1029/2008JB006132, b02212, 2009.

Hill, R.: The Elastic Behaviour of a Crystalline Aggregate, Proc. Phys. Soc. London, Sect. A, 65, 349, doi:10.1088/0370-1298/65/5/307, 1952.

Hofstede, C., Eisen, O., Diez, A., Jansen, D., Kristoffersen, Y., Lambrecht, A., and Mayer, C.: Investigating englacial reflections with vibro- and explosive-seismics surveys at Halvfarryggen ice dome, Antarctica, Ann. Glaciol., 54, 189–200, doi:10.3189/2013AoG64A064, 2013.

Hofstede, C., Christoffersen, P., Hubbard, B., Doyle, S. H., Young, T. J., Diez, A., Eisen, O., and Hubbard, A.: Physical Conditions of Fast Glacier Flow: 2. Variable Extent of Anisotropic Ice and Soft Basal Sediment From Seismic Reflection Data Acquired on Store Glacier, West Greenland, J. Geophys. Res., doi:10.1002/2017JF004297, 2018.

Horgan, H. J., Anandakrishnan, S., Alley, R. B., Peters, L. E., Tsoflias, G. P., Voigt, D. E., , and Winberry, J. P.: Complex fabric development revealed by englacial seismic reflectivity: Jakobshavn Isbræ, Greenland, Geophys. Res. Lett., 35, 1–6, doi:10.1029/2008GL033712, 2008.

Horgan, H. J., Anandakrishnan, S., Alley, R. B., Burkett, P. G., and Peters, L. E.: Englacial seismic reflectivity: imaging crystal-orientation fabric in West Antarctica, J. Glaciol., 57, 639–650, doi:10.3189/002214311797409686, 2011.

Kerch, J.: Crystal-orientation fabric variations on the cm-scale in cold Alpine ice: Interaction with paleo-climate proxies under deformation and implications for the interpretation of seismic velocities, Ph.D. thesis, Ruprecht-Karls-Universität Heidelberg, doi:10.11588/heidok.00022326, http://epic.awi.de/42799/, 2016.

Kerch, J., Eichler, J., Weikusat, I., and Eisen, O.: Eigenvalues of crystal-orientation tensors for c-axes distributions of vertical thin sections from the Alpine ice core KCC (2013), doi:10.1594/PANGAEA.864228, 2016a.

Kerch, J., Weikusat, I., Jansen, D., and Eisen, O.: Crystal c-axes (fabric analyser G50) of ice core samples (vertical thin sections) collected from the Alpine ice core KCC (2013), doi:10.1594/PANGAEA.864226, 2016b.

Mainprice, D., Hielscher, R., and Schaeben, H.: Calculating anisotropic physical properties from texture data using the MTEX open-source package, Geological Society, London, Special Publications, 360, 175–192, doi:10.1144/SP360.10, 2011.

Martin, C., Gudmundsson, G., Pritchard, H., and Gagliardini, O.: On the effects of anisotropic rheology on ice flow, internal structure, and the age-depth relationship at ice divides, J. Geophys. Res., 114, 1–18, doi:10.1029/2008JF001204, 2009.

Maurel, A., Lund, F., and Montagnat, M.: Propagation of elastic waves through textured polycrystals: application to ice, Proc. Roy. Soc. London, Ser. A, 471, doi:10.1098/rspa.2014.0988, 2015.

Mikesell, T. D., van Wijk, K., Otheim, L. T., Marshall, H.-P., and Kurbatov, A.: Laser Ultrasound Observations of Mechanical Property Variations in Ice Cores, Geosciences, 7, doi:10.3390/geosciences7030047, 2017.

Montagnat, M., Azuma, N., Dahl-Jensen, D., Eichler, J., Fujita, S., Gillet-Chaulet, F., Kipfstuhl, S., Samyn, D., Svensson, A., and Weikusat, I.: Fabric along the NEEM ice core, Greenland, and its comparison with GRIP and NGRIP ice cores, The Cryosphere, 8, 1129–1138, doi:10.5194/tc-8-1129-2014, 2014.

Nanthikesan, S. and Sunder, S. S.: Anisotropic elasticity of polycrystalline ice Ih, Cold Reg. Sci. Technol., 22, 149–169, doi:10.1016/0165-232X(94)90026-4, 1994.

Oerter, H., Drücker, C., Kipfstuhl, S., and Wilhelms, F.: Kohnen Station the Drilling Camp for the EPICA Deep Ice Core in Dronning Maud Land, Polarforschung, 78, 1–23, 2009.

Peternell, M., Kohlmann, F., Wilson, C. J. L., Seiler, C., and Gleadow, A. J. W.: A new approach to crystallographic orientation measurement for apatite fission track analysis: Effects of crystal morphology and implications for automation, Chem. Geol., 265, 527–539, doi:10.1016/j.chemgeo.2009.05.021, 2009.

Pettit, E. C., Thorsteinsson, T., Jacobson, H. P., and Waddington, E. D.: The role of crystal fabric in flow near an ice divide, J. Glaciol., 53, 277–288, doi:10.3189/172756507782202766, 2007.

Picotti, S., Vuan, A., Carcione, J. M., Horgan, H. J., and Anandakrishnan, S.: Anisotropy and crystalline fabric of Whillans Ice Stream (West Antarctica) inferred from multicomponent seismic data, J. Geophys. Res., 120, 4237–4262, doi:10.1002/2014JB011591, 2015.

Seddik, H., Greve, R., Placidi, L., Hamann, I., and Gagliardini, O.: Application of a continuum-mechanical model for the flow of anisotropic polar ice to the EDML core, Antarctica, J. Glaciol., 54, 631–642, doi:10.3189/002214308786570755, 2008.

Smith, E. C., Baird, A. F., Kendall, J. M., Martín, C., White, R. S., Brisbourne, A. M., and Smith, A. M.: Ice fabric in an Antarctic ice stream interpreted from seismic anisotropy, Geophys. Res. Lett., 44, 3710–3718, doi:10.1002/2016GL072093, 2017.

Sunder, S. S. and Wu, M. S.: Crack nucleation due to elastic anisotropy in polycrystalline ice, Cold Reg. Sci. Technol., 18, 29–47, doi:10.1016/0165-232X(90)90036-V, 1990.

Tsvankin, I.: Seismic signatures and analysis of reflection data in anisotropic media, Pergamon, 2001.

Vaughan, M. J., van Wijk, K., Prior, D. J., and Bowman, M. H.: Monitoring the temperature-dependent elastic and anelastic properties in isotropic polycrystalline ice using resonant ultrasound spectroscopy, The Cryosphere, 10, 2821–2829, doi:10.5194/tc-10-2821-2016, 2016.

Vaughan, M. J., Prior, D. J., Jefferd, M., Brantut, N., Mitchell, T. M., and Seidemann, M.: Insights into anisotropy development and weakening of ice from in situ P wave velocity monitoring during laboratory creep, J. Geophys. Res., pp. n/a–n/a, doi:10.1002/2017JB013964, 2017JB013964, 2017.

Voigt, W.: Lehrbuch der Kristallphysik: mit Ausschluss der Kristalloptik, 1910.

Weikusat, I., Kipfstuhl, S., and Lambrecht, A.: Crystal c-axes (fabric G20) of ice core samples collected from the EDML ice core with links to raw data files, doi:10.1594/PANGAEA.807207, 2013a.

Weikusat, I., Kipfstuhl, S., and Lambrecht, A.: Crystal c-axes (fabric G50) of ice core samples collected from the EDML ice core with links to raw data files, doi:10.1594/PANGAEA.807206, 2013b.

Weikusat, I., Lambrecht, A., and Kipfstuhl, S.: Eigenvalues of crystal orientation tensors for c-axes distributions of horizontal thin sections from the EDML ice core, doi:10.1594/PANGAEA.807141, 2013c.

Weikusat, I., Lambrecht, A., and Kipfstuhl, S.: Eigenvalues of crystal orientation tensors for c-axes distributions of vertical thin sections from the EDML ice core, doi:10.1594/PANGAEA.807142, 2013d.

Weikusat, I., Jansen, D., Binder, T., Eichler, J., Faria, S. H., Wilhelms, F., Kipfstuhl, S., Sheldon, S., Miller, H., Dahl-Jensen, D., and Kleiner, T.: Physical analysis of an Antarctic ice core – towards an integration of micro- and macrodynamics of polar ice, Philos. Trans. R. Soc. London, Ser. A, 375, doi:10.1098/rsta.2015.0347, 2017.

Wilson, C. J. L., Russell-Head, D. S., and Sim, H. M.: The application of an automated fabric analyzer system to the textural evolution of folded ice layers in shear zones, Ann. Glaciol., 37, 7–17, doi:10.3189/172756403781815401, 2003.

Woodcock, N. H.: Specification of fabric shapes using an eigenvalue method, Geol. Soc. Am. Bull., 88, 1231–1236, 1977.

Table 2. Summary of the results from the seismic velocity comparison between frameworks. Values are calculated depth-profile average (with standard deviation) and/or extreme (±) interval velocity differences (other than RMS) for incidence angles of 0 – 70°. Negative values indicate smaller velocities from the *cx* framework relative to the *ev* framework. ~~Extreme~~ The reported extreme values can be influenced by outliers from the general trend.~~Reading example (*): For a specific seismic plane azimuth ϑ_s, an incidence angle ψ and a specific interval at the KCC site the SV-wave velocity as calculated with the *cx* framework is found to be 279 ms^{-1} higher than is calculated with the *ev* framework which is the maximum difference for any combination of ϑ_s, ψ and depth.~~

Description	Notation	EDML	KCC
V-R bounds for *cx* framework	$\Delta v_{p0}^{cx} = v_{p0}^{cx} - v_{p0}^{cx,R}$	22.3 ± 4.5 ~~ms^{-1}~~ m s^{-1}	20.9 ± 6.0 ~~ms^{-1}~~ m s^{-1}
Difference between framework velocities at vertical incidence	$\Delta v_{p0} = v_{p0}^{cx} - v_{p0}^{ev}$	2 ± 23 ~~ms^{-1}~~ m s^{-1}, $-74/+90$ ~~ms^{-1}~~ m s^{-1}	-47 ± 25 ~~ms^{-1}~~ m s^{-1}, min. -135 ~~ms^{-1}~~ m s^{-1}
	$\Delta v_{sh0} = v_{sh0}^{cx} - v_{sh0}^{ev}$	-2 ± 22 ~~ms^{-1}~~ m s^{-1}, $-49/+55$ ~~ms^{-1}~~ m s^{-1}	9 ± 15 ~~ms^{-1}~~ m s^{-1}
	$\Delta v_{sv0} = v_{sv0}^{cx} - v_{sv0}^{ev}$	-9 ± 43 ~~ms^{-1}~~ m s^{-1}, $-115/+110$ ~~ms^{-1}~~ m s^{-1}	65 ± 42 ~~ms^{-1}~~ m s^{-1}, max. 212 ~~ms^{-1}~~ m s^{-1}
Difference between zero-offset RMS velocities at bedrock	$v_{p0,rms}^{cx} - v_{p0,rms}^{ev}$	0 (cancels out due to systematic bias)	-39 ~~ms^{-1}~~ m s^{-1}
		~~-18m~~ -18 ~~s^{-1}~~ m s^{-1} at 750 ~~m~~ m depth	
	$v_{sv0,rms}^{cx} - v_{sh0,rms}^{cx}$	59 ~~ms^{-1}~~ m s^{-1}	45 ~~ms^{-1}~~ m s^{-1}
	$v_{sv0,rms}^{ev} - v_{sh0,rms}^{ev}$	67 ~~ms^{-1}~~ m s^{-1}	no ~~SWS~~ shear-wave splitting
Difference between framework velocities at non-vertical incidence	$v_p^{cx,\vartheta_s}(\psi) - v_p^{ev}(\psi)$	$-84/+131$ ~~ms^{-1}~~ m s^{-1}	± 185 ~~ms^{-1}~~ m s^{-1}
	$v_{sh}^{cx,\vartheta_s}(\psi) - v_{sh}^{ev}(\psi)$	$-184/+86$ ~~ms^{-1}~~ m s^{-1}	~~$-100/+65$m~~ $-91/+65$ ~~s^{-1}~~ m s^{-1}
(*)	$v_{sv}^{cx,\vartheta_s}(\psi) - v_{sv}^{ev}(\psi)$	~~$-142/+215$m~~ $-142/+168$ ~~s^{-1}~~ m s^{-1}	$-273/+279$ ~~ms^{-1} (*)~~ m s^{-1}
Change of *cx* velocity with azimuth ϑ_s	$v_p^{cx,\vartheta_s}(\psi) - v_p^{cx,\vartheta_s=0}(\psi)$	$-97/+150$ ~~ms^{-1}~~ m s^{-1}	$-194/+109$ ~~ms^{-1}~~ m s^{-1}
	$v_{sh}^{cx,\vartheta_s}(\psi) - v_{sh}^{cx,\vartheta_s=0}(\psi)$	$-73/+50$ ~~ms^{-1}~~ m s^{-1}	± 65 m s^{-1}
	$v_{sv}^{cx,\vartheta_s}(\psi) - v_{sv}^{cx,\vartheta_s=0}(\psi)$	$-210/+191$ ~~ms^{-1}~~ m s^{-1}	$-231/+273$ m s^{-1}
Shear-wave splitting	$v_{sv}^{cx,\vartheta_s}(\psi) - v_{sh}^{cx,\vartheta_s}(\psi)$	max. 281 ~~ms^{-1}~~ m s^{-1}	max. 281 ~~ms^{-1}~~ m s^{-1}
Change of shear-wave splitting with azimuth ϑ_s	$\Delta_\vartheta \left(v_{sv}^{cx} - v_{sh}^{cx}\right)$	$-177/+216$ ~~ms^{-1}~~ m s^{-1}	$-269/+239$ ~~ms^{-1}~~ m s^{-1}
Variability (std. dev.) of *ev* framework velocity	$s(v_{p0}^{ev})$	10–49 ~~ms^{-1}~~ m s^{-1} (depending on depth interval)	17 ~~ms^{-1}~~ m s^{-1} (detrended)
Variability (std. dev.) of *cx* framework velocity	$s(v_{p0}^{cx})$	20–37 ~~ms^{-1}~~ m s^{-1} (depending on depth interval)	17 ~~ms^{-1}~~ m s^{-1} (detrended)
Vertical change (between 10 cm samples) in *cx* velocity	δv_{p0}^{cx}	$\sim \pm 50$ ~~ms^{-1}~~ m s^{-1} (high resolution intervals)	$-46/+64$ ~~ms^{-1}~~ m s^{-1}
	δv_{sh0}^{cx}		± 54 ~~ms^{-1}~~ m s^{-1}